Facile Hydrothermal Synthesis of Hierarchically Mesoporous Nickel-Cobalt Selenide (NiCoSe) Nanowires for High Performance Supercapacitors

By

Muhammad Waqar

School of Chemical and Materials Engineering

National University of Sciences and Technology

2022

Facile Hydrothermal Synthesis of Hierarchically Mesoporous Nickel-Cobalt Selenide (NiCoSe) Nanowires for High Performance Supercapacitors

Muhammad Waqar
Reg. No: NUST2020MSE15-00000330779

This thesis is submitted as a partial fulfilment of the requirements for the degree of

MS in (Materials and Surface Engineering)

Supervisor Name: Dr. Aftab Akram

School of Chemical and Materials Engineering (SCME)
National University of Sciences and Technology (NUST)
H-12 Islamabad, Pakistan

June, 2022

Dedication

I dedicate this thesis to my loving and caring Mother and my beloved Father.

Acknowledgments

All admiration to Allah Almighty. He is the One, who bestows and gives the power to us to think, utilize our expertise in knowledge in achieving remarkable solutions for mankind in every field. Therefore, I express my greatest thanks to Almighty Allah the universal and the architect of the world. Allah Almighty says in Quran:

“Read! In the name of your lord” (Alaq; 1st revealed ayah)

This Quranic verse sums up the entire importance of education in the lives of humans.

I like to express my gratefulness to my very nice and respected supervisor Dr. Muhammad Aftab Akram for their clear and patient guidance that directed me to fulfill my project and this thesis. Their cool and calm behavior motivated me to do my best. Their valuable suggestions and feedback contributed to this thesis. Also, I am very grateful to all my teachers who helped me and motivated me to do my best. I would also like to thank my parents, family members and friends for their help, prayers, and their valuable suggestions

I want to thank Dr Zeeshan Ali for his continuous support and motivation which helped me at various stages during my Masters.

I also want to thank Mr. Tayyab Ahsan and Ali Arshad for their support as they helped a lot during characterization and lab work.

I acknowledge the support provided by the Materials Engineering department of SCME for providing me a platform to perform my experiments and using my skills in research work.

My biggest appreciation to Saqlain (NG staff member), who assisted me in all the possible manners.

I acknowledge the financial aid and technical assistance provided by our department, SCME, during my research experience and made this project work memorable forever.

Lastly, I would like to thank my family for their support and prayers.

-Muhammad Waqar

Abstract

Hierarchical mesoporous Nano-wires nickel-cobalt oxide at nickel cobalt selenide (core/ shell) has been established as a promising electrode material due to the synergic enhancement effect of cobalt cations replacement with selenium and nickel. NCSe//NCO (Core/shell) nanowires were synthesized using a facile hydrothermal approach followed by annealing treatment. For a comparative study nickel cobalt oxide (NCO) was also synthesized by the same method. Electrochemical analysis affirmed the developed hierarchically mesoporous NCSe//NCO nanowires for supercapacitors. NCSe //NCO nanowires exhibit specific capacitance of 3281.54 F g^{-1} at 1 Ag^{-1}. Moreover, asymmetric testing by employing NCSe //NCO as positive electrode and Activated Carbon as a negative electrode. An asymmetric supercapacitor (ASC) with activated carbon shows high energy density 37.91 Wh kg^{-1} at a power density of 749.95W kg^{-1} and excellent capacitance retention of 116% over 7000 cycles with columbic efficiency of 99% at 20 Ag^{-1}.

Table of Contents

List of Figures

List of Tables

List of Abbreviations

CO	_____	Cobalt Oxide
NCO	_____	Nickel Cobalt Oxide
NCO//NCSE	_____	Nickel cobalt oxide//nickel cobalt selenide core/shell
CV	_____	Cyclic Voltammetry
GCD	_____	Galvanic Charge Discharge

Chapter 1

Introduction

1.1 Introduction

The world is facing a severe energy crisis. The need of great importance is to move towards sustainable and efficient green energy resources [1]. Because of expanded human populace and development in energy utilization, the world's energy resources are draining step by step. The reliance on petroleum products like coal gas and normal oil is surpassing a disturbing rate. Because of this, petroleum derivatives are depleting excessively. Additionally, the consuming of these materials produces gases like CO2, SOx and NOx which are causing contamination in the climate as well as a hazard for life on Earth due to global warming and greenhouse effect also, environmental and water pollution has become so fatal for human life. This pollution is becoming detrimental to human health [2] . Heavy metals and organic dyes are among the list of materials which pollute the environment and cause serious health issues. Since the capacity of automatic cleaning is limited and untreated industrial waste is also thrown into these water bodies, water pollution has become a natural phenomenon in the world. Now there is a crucial need to maintain a green and cleaner environment.

The renewable energy resources have been focused on overcoming the energy crisis with depletion of nonrenewable energy resources like fossil fuels and petroleum. Many materials are being tested that are not only cost-effective but also generate renewable energy[3]. It is urgent for us to develop environmentally friendly and green technologies so there would be lesser contamination in the environment. There have been production of several materials and devices in the last few decades that are eco-friendly and able to produce renewable energy along with the ability of storing it for a long time, these include solar cells, fuel cells, supercapacitors etc. [4-7]. Higher energy and power density are required due to increased energy usage and dependence on portable energy devices[8, 9].

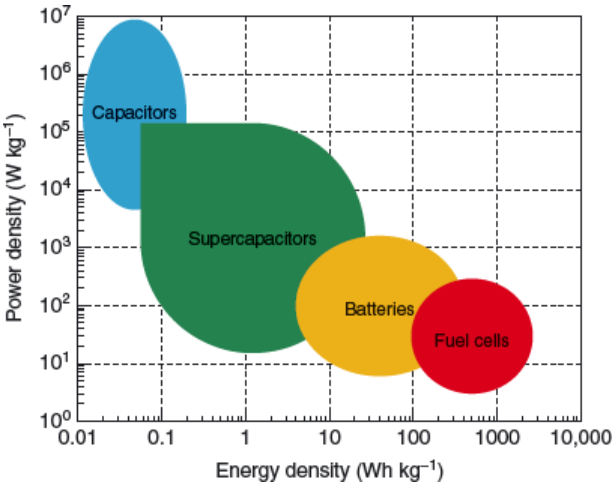

figure 1.1 Rangone plot of energy storage devices [10]

1.2 Renewable Energy Resources

Renewable energy resources are those which cut off our dependence on non-renewable energy resources. These resources do not deplete, and they can be reused again for our convenience. There are many forms of renewable energies which include:

- Hydrothermal energy[11]
- Geothermal energy[12]
- Solar energy[13, 14]
- Wind energy [15]
- Biomass[16, 17]

Renewable energy sources should be used as they are natural and better. They are also cost-effective and 'green.' They do not create havoc for the environment. They are getting cheaper by the day as technology is progressing. New technologies are also being explored in them.

1.3 Energy Storage devices

Increase in the demand for energy and more renewable resources developed there is a strong need for devices which can store energy. Energy storage systems are becoming more necessary as the availability of renewable energy sources rises. [18].

Energy storage systems are divided into five major categories

- Mechanical system
- Chemical system
- Electrochemical system
- Electrical system
- Thermal system [19]

The most common energy storage devices that come in electrochemical and electrical systems are

- Batteries
- Supercapacitors

table 1.1 Characteristics of energy storage devices [6]

Characteristics	Capacitor	Supercapacitor	Battery
Specific energy ($W\,h\,kg^{-1}$)	< 0.1	1–10	10–100
Specific power ($W\,kg^{-1}$)	$\geqslant 10,000$	500–10,000	< 1000
Discharge time	10^{-6} to 10^{-3}	s to min	0.3–3 h
Charge time	10^{-6} to 10^{-3}	s to min	1–5 h
Coulombic efficiency (%)	About 100	85–98	70–85
Cycle-life	Almost infinite	$> 500,000$	about 1000

table 1.2 Comparison of batteries and supercapacitors [6]

Comparison parameter	Battery	Supercapacitor
Storage mechanism	Chemical	Physical
Power limitation	Reaction kinetics, mass transport	Electrolyte conductivity
Energy storage	High (bulk)	Limited (surface area)
Charge rate	Kinetically limited	High, same as discharge
Cycle life limitations	Mechanical stability, chemical reversibility	Side reactions

1.4 Batteries

The primary kind of electrochemical cell-based energy storage is found in batteries. It can store energy through reversible electrochemical reactions. It can charge and discharge several times when the load is applied. Major types of batteries include

- Primary Batteries
- Secondary Batteries
    - Lead-acid batteries [20]
    - Li-ion batteries
    - Sodium-ion
    - Li-polymer
    - Li Sulphur
    - Flow

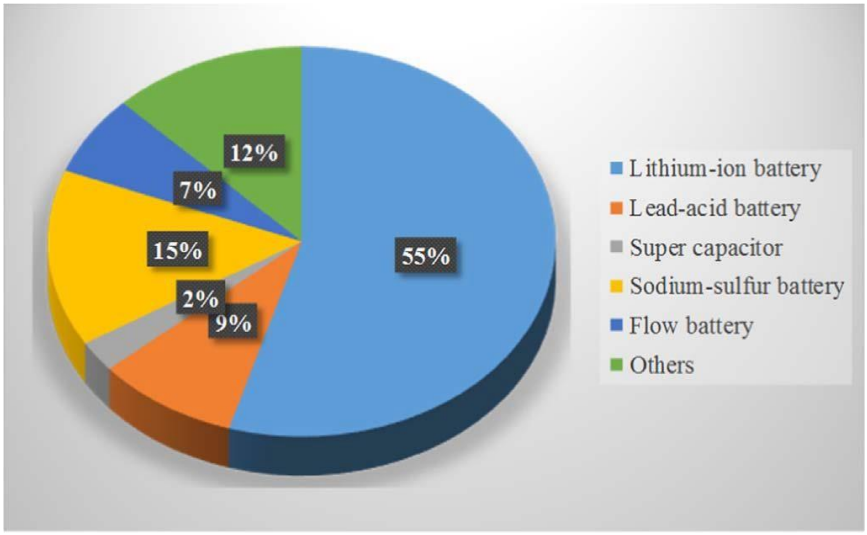

figure 1.2 Energy storage system globally [21]

1.5 Supercapacitors

Supercapacitors (SC) are an electrochemical device that has gained quite consideration within the previous decade due to their superior electrical energy storage and

conversion capabilities. At the electrolyte electrode interface, these devices feature nanoscopic charge separation[22]. These devices provide a link between traditional electrolytic capacitors and rechargeable batteries by demonstrating capacitor power density and battery storage capacity [23]. Supercapacitors are being used as they are able to retain more energy and have a prolonged expectancy cycle. The specific capacitance is calculated as follows:

$$Q = CV \ldots\ldots\ldots\ldots\ldots\ldots (1)$$

Where,

C stands for specific capacitance, V for operating window, and Q for stored charge. Because of its high power output and low cost, SCs are considered to be a good choice for energy storage. They are divided into two groups based on the materials' compositions.

1.6 Types of Supercapacitors

1.6.1 Conventional Capacitors

Two electrodes and a dielectric medium separate the two electrodes in a capacitor. In Figure 1.3, By putting a voltage across the plates, the electric field in the dielectric material creates equal-sized negative and positive charges on both sides. The formula for computing capacitance (C), which is measured in farads (F) and used to describe how energy is stored in capacitors, is

$$\boldsymbol{c = \frac{A \times \varepsilon}{d}} \ldots\ldots\ldots\ldots\ldots\ldots (2)$$

Here

A is the surface area, ϵ is the dielectric constant, d is the Separation distance

Traditional capacitors can store energy in the pico to microfarad range.

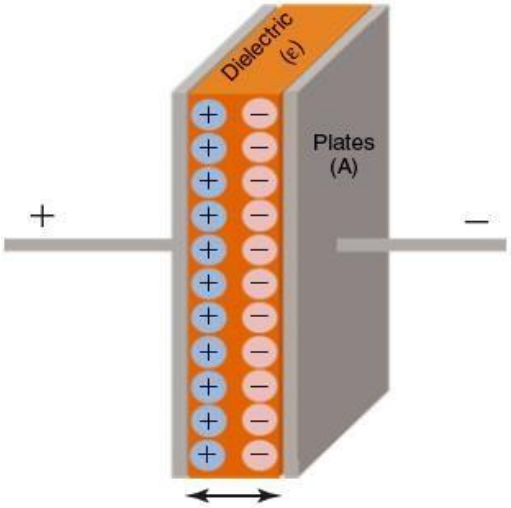

figure 1.3 Structure of Conventional Capacitor [10]

Supercapacitors are categorized into three following types:

Electric double layer capacitors	▪ Carbon aerogels ▪ Activated carbons ▪ Carbon fibers ▪ Carbon nanotubes
Pseudo-capacitors	▪ Metal oxides ▪ Conducting polymers
Hybrid capacitors ❑ **Asymmetric** ❑ **Composite** ❑ **Battery-type**	▪ Carbon materials, conducting polymers ▪ Carbon materials, metal oxides

figure 1.4 Supercapacitors types [24]

1.6.2 Electron Double Layer Supercapacitors (EDLC)

The functioning of an EDLC is identical to that of a typical capacitor, with the exception that an electrode-electrolyte interface is used for charge storage rather than a dielectric material, as illustrated in Figure. With no redox reaction and no faradic reaction, the charge storage mechanism in EDLC is entirely physical, meaning that

there is no active electrode material. Because of the physical charge transfer, EDLC has a long cycle life. The capacitance of an EDLC can be written as

$$C = \frac{A\varepsilon}{4\pi d} \qquad \text{..... (3)}$$

Where

A denotes electrodes Surface area

ϵ denotes dielectric constant

D denotes effective thickness of the double layer

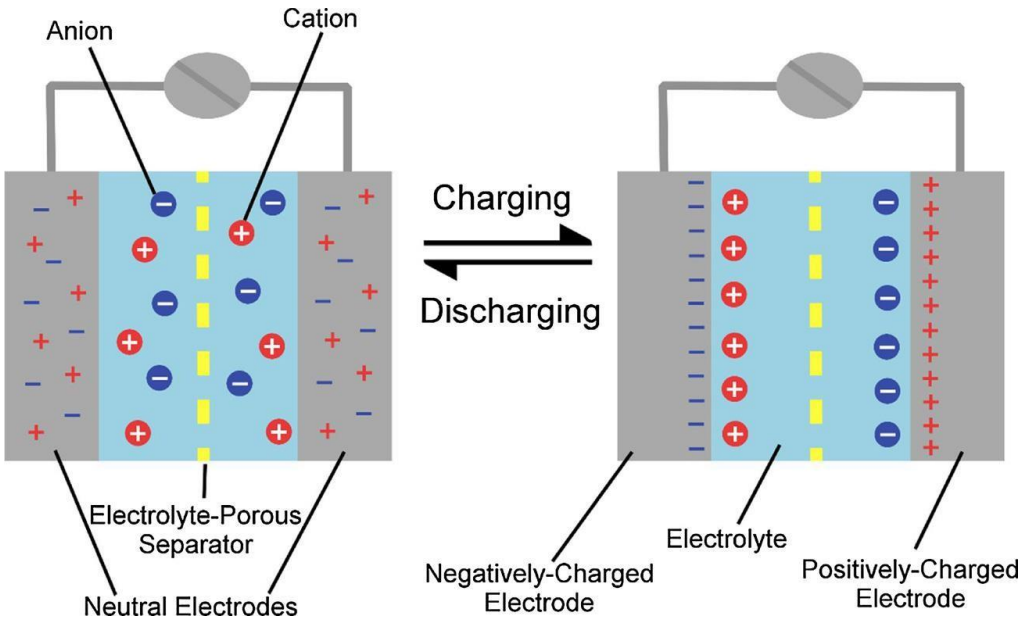

figure 1.5 EDLC's charge storing mechanism [5]

1.6.3 Pseudocapacitors

Redox reactions are used to store charges. These capacitors utilize conductive polymers, transition metal hydroxides, and oxides. The faradic charge transfer process or intercalation and electrosorption are used to induce capacitance [25] [26]

1.6.3.1 Advantages

- High energy density

- Large specific capacitance
- Low price

1.6.3.2 Shortcomings:

- Low rate capability
- Less Stable
- Semiconductors obstruct faster electron transport for large charge/discharge cycles.

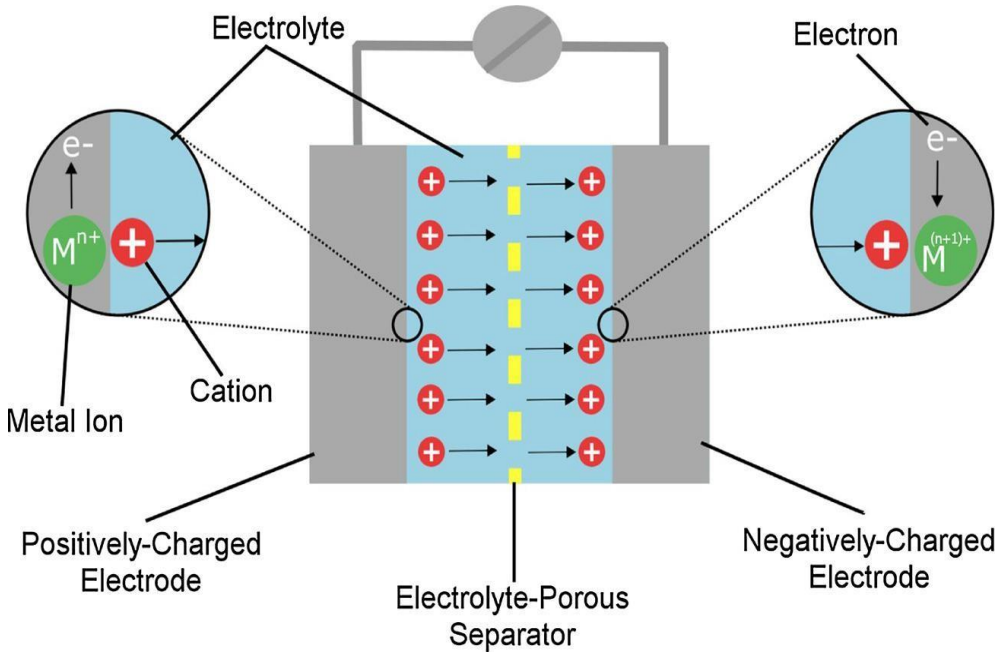

figure 1.6 Pseudo capacitor charge storage mechanism [5]

1.6.4 Hybrid Supercapacitors

- Hybrid supercapacitors combine EDLC and Pseudocapacitor technology as shown in figure 1.7. Hybrid supercapacitors are classified as either symmetric or asymmetric, with the positive electrode being a pseudo capacitor and the negative electrode being EDLC. Hybrid supercapacitors have the following key characteristics:
- Excellent specific capacitance

- High Power Density
- Greater Energy Density
- Superior cyclic stability

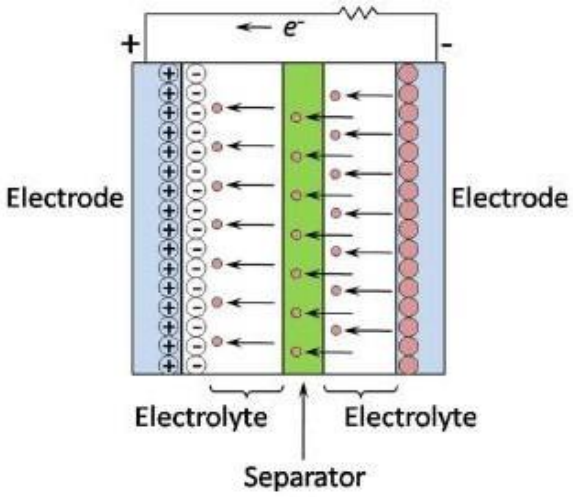

figure 1.7 Mechanism in hybrid Supercapacitor [24]

1.7 Components of Supercapacitors

1.7.1 Electrode Materials

High-performance SCs are the focus of nanostructured materials. It is highly dependent on surface area since it directly affects the working of capacitance. When a material's capacitance is high, it suggests it has a lot of porosity and pore volume for a given surface area. A supercapacitor's storage performance is heavily influenced by the electrode materials. Supercapacitors are categorized into three groups according to the electrode material being used, which includes electrochemical double layered capacitor (EDLC), pseudo capacitors, and hybrid capacitors. Other carbon materials such as graphene, carbon nanotubes (CNTs), and activated carbon also display EDLC characteristics. While the electrode materials themselves are electrochemically inactive, the charge storage only happens because of the deposition of charges/ions on the surface of electrode materials. On the other hand, the highly redox active transition metal oxides and chalcogenides belong to the pseudocapacitive class, where charge is held in reserve as a result of oxidation reduction reaction on the electrode surface. The

various primary electrode materials consist of

1.7.2 Carbon Materials

These materials are the most commonly utilized in supercapacitors owing to their ease of processing and high abundance and being inexpensive. In CV, these materials have a nearly rectangular shape, while in GCD, they have a linear curve. The majority of electrode materials fall within this category.

1.7.2.1 Activated Carbon

Supercapacitors are most often made with activated carbon. In comparison to carbon nanotubes and graphene, activated carbon has a greater surface area and is less expensive. Natural resources are used to obtain its predecessors. The carbonization procedure, which is a heat treatment method carried out in an inert atmosphere, can be used to activate precursors.

1.7.2.2 Carbon nanotubes (CNTs)

CNTs are manufactured from the decomposition of hydrocarbons and are a versatile material for electrochemical devices. SWCNTs or MWCNTs can be synthesized depending on the technique. CNTs have great conductivity and surface area, along with outstanding mechanical and chemical properties. The electrode made of CNTs has almost the same capacitance as an electrode made of activated carbon, indicating that supercapacitors made from CNTS capitalize their surface area.

1.7.2.3 Graphene

In the recent decade, researchers have focused intensively on graphene due of its excellent qualities, which are essential for high-performance energy applications. Graphene is a material that has a number of desirable properties.

- Remarkable surface area
- Lighter Weight
- Extraordinary conductivity [27]
- Superior Mechanical Strength

- Greater Charge Mobility
- Better efficiency
- Affordability

1.7.3 Conducting Polymers

Due to redox reactions, conducting polymers exhibit pseudo capacitance behaviour. When ions are transported to a polymer, oxidation occurs, whereas reduction happens when the polymer releases the ions into an electrolyte. For the supercapacitor applications, the usage of conduction polymer for an electrode material has various advantages.

- Economical
- Eco-friendly
- excellent conductivity
- large working window
- Large Surface Area
- Large Capacitance value
- Low Equivalent Resistivity and Conductivity

CPs that are commonly utilised for electrode materials include

1.7.3.1 Polyaniline

Polyaniline (PANI) is a conducting polymer that, in addition to carbon-based materials, is used in SCs as they are inexpensive, possess high specific capacitance, flexibility, and ease of manufacturing. The most significant issue that restricts PANI's use is its inability to maintain stability and degradation at a high rate. As a result, combining PANI with different materials improves its stability. PANI is made by polymerizing aniline monomer with ammonium persulfate or iron chloride as an oxidant [28-31].

1.7.3.2 Polypyrrole (PPy)

Polypyrrole (PPy) is a conducting polymer that's utilised in many electronic devices. Easy production, good redox activity, lower density, and high conductivity are all advantages of PPy. When compared to EDLC, it can store a larger amount of charge. The concentration of dopant impacts the stability and capacitance performance of PPy and can be synthesised by chemical polymerization employing an oxidising agent. [26, 32, 33]

1.7.4 Metal Oxides

Metal oxides are an excellent choice to be employed as the electrode materials for energy storage applications because of their high specific capacitance and high level of stability. Due to their enormous energy density, and tremendous electrochemical performance they have attracted the attention of researchers. There are some requirements that must be completed before a metal oxide may be considered for use in an electrochemical supercapacitor.

- Metal oxide should be conductive
- protons can sweep into the lattice of oxide during reduction
- Existence or coexistence of two or three oxidation states

Vanadium oxide, Nickel oxide, Cobalt oxide, Iron oxide, and Manganese oxide are examples of typical oxide materials that match fundamental requirements and are employed as supercapacitors due to their excellent qualities. [34-37]

1.7.5 Metal Chalcogenides

Due to their anisotropic feature, the industrially important and scientifically noteworthy metal chalcogenides have extensively been explored in the past two decades. Transition elements including S, Se, and Te, mixed with VI A group elements to generate dual stable layered crystalline structures. They are commonly used in SCs because of their good features, which include:

• Have longer life cycle
• They are flexible

• Provide extra active sites and catalytic activity
• Augment the conductivity and reduce its internal resistance and ohmic loss
• Have shorter pathway for transportation of electrons.

Because of their exceptional qualities, nickel selenide, cobalt selenide, molybdenum diselenide, copper sulphide, molybdenum sulphide, nickel sulphide, and cobalt sulphide are extensively utilised metal chalcogenides for supercapacitor electrode material.

1.7.5.1 Nickel Selenides

Am Nickel selenides have gotten a lot of attention among the transition metal chalcogenides because of their tuneable electronic configuration and numerous oxidation states. Their paramagnetic nature, which gives them a resistance of 10^{-3}ohm.cm^{-1}, makes them ideal candidates for energy storage, particularly supercapacitors.

1.7.5.2 Cobalt selenides

Because of the following properties, cobalt selenides have piqued interest as a promising Transition Metal Selenide for supercapacitor applications:

• Exceptional chemical stability
• Easy to fabricate
• Cheap
• Their availability in a variety of oxidation states, including CoSe, $CoSe_2$, and non-stoichiometric $Co_{0.85}Se$.

1.7.6 Molybdenum Diselenide

Molybdenum Diselenide (MoSe2) is an inexpensive, abundant material with a high capacitance. The robust covalent interactions which characterise the Se-Mo-Se interrelation compress the molybdenum atom sandwiched between two selenium atoms in $MoSe_2$. Weak van der Waals forces, which are accountable for ion relocation in the Charge Discharge procedure, hold the stacked layers together. Only a few studies on $MoSe_2$ for SC applications have been published.

1.7.7 Nickel Sulfides

Owing to the excellent physicochemical properties they possess, nanometer-sized metal sulphides have become increasingly important in electronics, particularly optical and optoelectronic devices in recent years. Nickel sulphide is certainly fascinating due to its various phases and morphologies, including NiS, Ni3S2, NiS2, Ni3S4, Ni7S10, and Ni9S8. Because nickel sulphides have a variety of phases and morphologies that cohabit as combinations of more than two distinct phases occasionally, researchers face the issue of attaining a uniform morphology with pure nickel sulphide.

1.7.7.1 Cobalt Sulfides

Cobalt sulphides have gotten a lot of interest in recently owing to their incredible qualities, which make them effective in a range of implementations such as super-capacitors (SCs), batteries, magnetic materials, etc. Although there has been a great amount of research on nanostructures of Cobalt Sulfides to be used as electrode materials for SCs, it is quite challenging to synthesize them without compromising their purity and complex morphology.
The difficulties could be linked to the following reasons.

- It is easy for Cobalt Sulfides to go through phase transformation as they exist in several chemical forms in nature.
- It is quite a challenge to synthesize high purity Cobalt Sulfides as they easily form bonds with oxygen due to their strong affinity to it, producing cobalt oxide and cobalt hydroxide.
- As they have a complex phase diagram, it is difficult to control the temperature.

1.7.8 Electrolytes

While fabricating a supercapacitor, our main concern is to improve its energy value which can be done in two of the following ways.

- Increasing the electrode material's capacitance
- widening the capacitor's operating potential.

Widening the working potential is more advantageous because it increases the device's energy density while also lowering the stacking numbers to achieve bigger potential differences. There has been a great deal of research into choosing an appropriate electrolyte material for super-capacitors because the cell voltage depends on the electrochemical stability of the electrolyte utilized. The electrolytes that have been developed, together with their respective potential windows, are listed below:

- Supercapacitors based on aqueous Electrolyte (1–1.3 V)
- Supercapacitors based on organic Electrolytes (2.5–2.7 V)
- Ionic Liquid Supercapacitors (3.5–4 V)

Ideal material for electrolyte would increase both, the energy density rates and life cycle and power output, reduce the internal resistance and decrease the self-discharge process. An ideal electrolyte should be light in mass, have high electrical conductivity, good electrochemical activity, and large tolerance towards degradation.

Types of Electrolytes

Electrolytes are divided three main types. Division of electrolytes can be explained via a flow diagram.

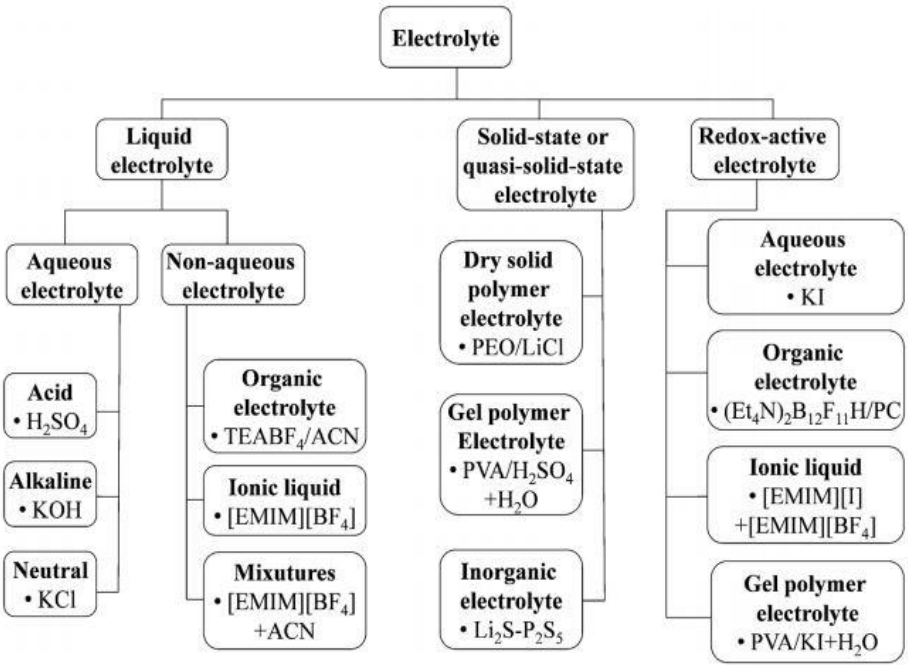

figure 1.8 Types of electrolytes

1.7.8.1 Liquid Electrolytes

The major part of developing a supercapacitor is the selection of its electrolytic material and hence there has been a great amount of research carried out on several liquid electrolytic materials. It is sub divided into two categories aqueous electrolytes and non-aqueous electrolyte. These liquid electrolytic materials are further classified into two groups that include Ionic Liquids and Organic electrolytes.

1.7.8.2 Aqueous Electrolytes

This group includes those electrolytes that are an aqueous solution of inorganic compounds and some salts. As they have separated ions, they are exceedingly conductive and hence quite effective in increasing the power density in an economical way due to the fact that they have lesser electrolytic resistance which helps in reducing the ESR value. Aqueous Electrolytes also have the advantage of being easily synthesized and handled, making them suitable to be used in supercapacitors.

1.7.8.2 Non-Aqueous Electrolytes

This type of electrolytes includes fused ions or organic salt solutions, these are quite effective to use as they don't degrade or decompose even at high working potential windows, they are also more durable than aqueous electrolytes and can be used in commercial applications. But they do have some disadvantages that are problematic when it comes to large scale production including their high cost, low conductivity, and toxicity. Non-aqueous electrolytes have the following categories:

1.7.8.2.1 Organic Electrolytes

A conducting salt is mixed with an organic solvent to make these. They are widely commercialized as they have a broad potential window (2.5–2.8 V) which helps in increasing the energy density and improving the thermal and cyclic stability of the device.

1.7.8.2.2 Ionic Electrolytes

In ionic liquids, an inorganic/organic anion is coupled with an asymmetric organic cation., they are made of salts having melting point less than 100 °C. To test their overall performance in a supercapacitor, they' frequently ingested in the original state

(without an impurity) or dissolved in organic solvents. These liquids are usually designed by choosing different cation-anion pairs with the aim of improving the functioning of potential window. The cations to be chosen include ammonium, phosphonium, pyrrolidinium etc. and anions include tetra*fl*uoroborate (BF4-).

1.7.8.2.3 Redox active Electrolytes

These are further divided into two types

Redox-active aqueous electrolytes

These electrolytes are quite special as they can increase the total capacitive functioning of supercapacitor appliance by extracting redox based capacitance from itself, unlike conventional supercapacitors which only relies on the oxidation, reduction reaction of the electrode. Some of these electrolytes include hydroquinones, KI, lignosulfonates, etc.

Redox-active non-aqueous electrolytes

Several non-aqueous electrolytes have been studied to enhance the cell voltage which would result in high energy density. These electrolytes include Organic and Ionic Liquid based electrolytes. The introduction of redox-active Polyfluorododecaborate cluster ions into an organic mixture solvent containing Propylene Carbonate and Dimethyl Carbonate, according to literature studies, would be extremely beneficial in enhancing the pseudocapacitive contribution of carbon-based supercapacitors.

Solid and Quasi-solid(Gel) Type Electrolytes:

These are gel electrolytes that are made up of a polymer matrix contained in a liquid electrolyte and are very flexible. They are appealing to employ because they aid in the fast miniaturization of electronic industries. Although liquid electrolytes offer superior ionic conductivity and hence facilitate redox reactions, their leakage and solution resistance limit their use on a broad scale and prevent them from being employed in portable electronic devices.

1.8 Applications of Supercapacitors

Currently, supercapacitors are widely used in

- Automobile industry [38]
- Hybrid transportation

- Grid stabilization
- Railway system
- Consumer electronics

Chapter 2

Literature Review

2.1 Literature Review

Supercapacitors in recent years have drawn more attention from the researchers. Having a lower energy density is a major problem for these devices besides this problem recent advancement in the electrode material and technology; they are filling the gap between the fuel cell and batteries. The figure 2.1 shows the material focused on recent years as well as the number of research work conducted on supercapacitors in the last two decades

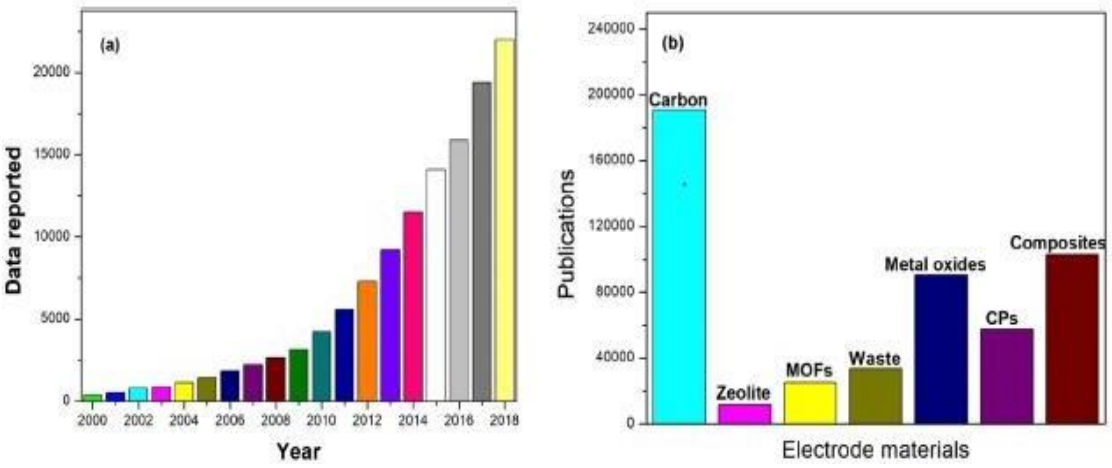

figure 2.1 (a) Number of research publication on supercapacitors 2000-2010 (b) Publications on electrode materials [39]

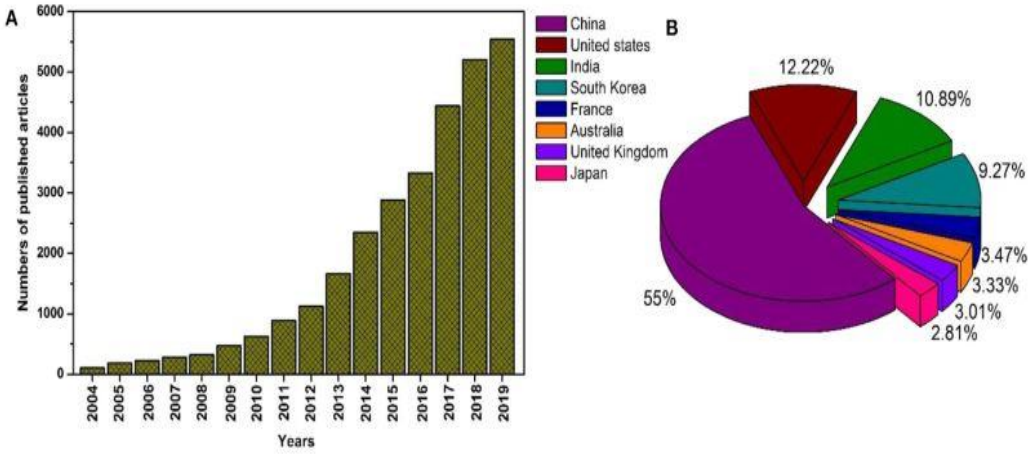

figure 2.2 (a) Number of research publication on supercapacitors 2004-2019 (b) country wise division of publications

2.2 Cobalt Oxide

It is discussed as a favorable material and there has been quite a lot of research on it. Specifically, it is explored in energy reserving devices like supercapacitors and batteries [39-41]. Cobalt oxides exist in four different forms, and among those, two of which are quite valuable for the energy storage applications.

Table 2.1 Types of cobalt oxide

Name	Formula
Cobalt (II) oxide	CoO
Cobalt (III) oxide	Co_2O_3
Cobalt (IV) oxide	CoO_2
Cobalt (II, III) oxide	Co_3O_4

The most commonly used form of Cobalt Oxide is Cobalt (II, III) oxide (CO) owing to its excellent capacitance and thermal properties [25], [42, 43]. CO is also an economical material and quite abundant. It possesses a spinal like structure which is illustrated in the figure. Co (II) ions are present. Red balls ions inhabit the tetrahedral 8(a) spots, while Co (III) ions take up the octahedral 16(d) positions. It has excellent

capacitance values, i.e., 3560 F g-1 for supercapacitors.

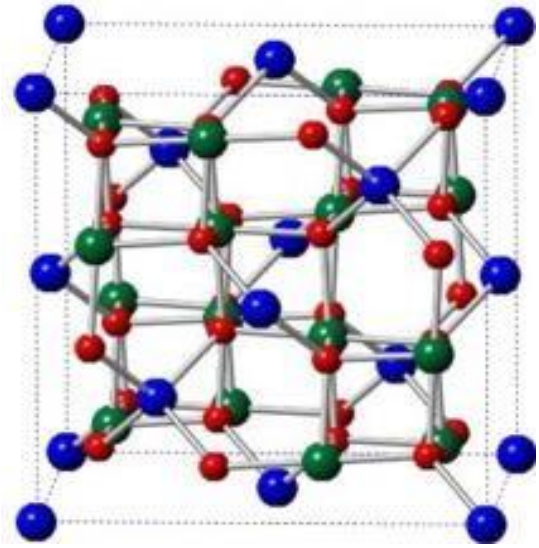

figure 2.3 The cystal structure of Cobalt (IV) oxide [39]

Despite the advantages, there are some drawbacks associated with CO, including its high resistivity, toxicity, and low charge ionic conductivity. Researchers are experimenting with numerous techniques to tackle this problem by creating a hybrid structure of CO. Graphene and carbon nanotubes are the most popular nanomaterials that have been used to synthesize hybrids and they can significantly enhance the charge transport and kinetics of the material, even when used in minute amount.

Poizot et al. used CO as an anode for the very the first time in lithium-ion battery in 2000 [34]. Alcántara et al., then reported $NiCo_2O_4$ as an electrode in sodium-ion batteries in March 2002 [44].

Tremendous study was conducted on the morphological properties for the supercapacitors as the capacitance value is interlinked with the morphology. Yuan YF et al. reported the synthesis 3D Co_3O_4 in March 2012, which consisted of a hierarchical crystal structure to be used for the pseudocapacitive applications. He grew nanoflakes film of about 20nm thickness which was porous in nature. The results showed that 443 F g^{-1} capacitance was achieved at 2 A g^{-1} [45]. Kang CW et al. in 2012 reported the synthesis of nanosheets of Co_3O_4 for the supercapacitor applications, for which he employed the electrodeposition method. He used Ti as a substrate for the growth of the nanosheets. The results showed that 1035 F g^{-1} was achieved for the specific capacitance at 2 A g^{-1} [46] Fin Y et al. in 2014 synthesized Co_3O_4 nanoflakes exhibiting a hierarchical crystal structure for the supercapacitor

applications. For its synthesis, he used precursor precipitation technique and the results demonstrated 896 F g^{-1} 1 A g^{-1} capacitance value and 79.2% capacitance retention at 40 A g^{-1} [47] Zhang G et al. in 2013 synthesized nanowires of Co_3O_4@ $NiCo_2O_4$ exhibiting a hierarchical structure for the supercapacitor applications. The results showed that an excellent value of aerial capacitance was achieved of about 1.97 F cm^{-2} at 4 mV s^{-1} and there was a capacitance retention after 1500 cycles of 83.7% [48]. Hu et al. in 2014 synthesized Co_3O_4@ MnO_2 having a hierarchal structure by employing hydrothermal method. The results revealed that a specific capacitance of about 560 F g^{-1} was achieved at 0.3 A g^{-1} and there was an excellent capacitance retention of about 95% even after 5000 cycles. [49]. W. Fu et al. in 2015 synthesized nano-flowers of $ZnCO_2O_4$ on Nickel foam to be employed for the supercapacitor application. The capacitance of 684.9 F g^{-1} was achieved at 1 A g^{-1} and there was around 95% of capacitance retention achieved following 3000 cycles [50]. C. Zhang et al. in 2015 synthesized nano-flowers of $NiCo_2O_4$ on graphene foam for application of supercapacitors, for which he utilized Chemical Vapor Deposition. The results showed that there was a specific capacitance of about1402 F g^{-1} at 1 A g^{-1} and 77% capacitance retention was achieved at 20 A g^{-1} after 5000 cycles [51]. Huixin Chen et al. in 2015 synthesized nano-sheets of $ZnNiCo_2O_4$ possessing a hierarchical structure. The results showed that a specific capacitance of 1728 F g^{-1} was attained at 1A g^{-1} and 1512 F g^{-1} at 15 A g^{-1} , while there was a capacitance retention of 87.5% at 20 A g^{-1} [52]. Wenquin et al. in 2015 studied the properties of hierarchical core-shell nanotubes of $ZnCo_2O_4/MnO_2$. The results showed that the material gave capacitance value of 1981 F g^{-1} at 5 A g^{-1}. Additionally, an asymmetric device was assembled, and the results were determined. The outcome revealed that the value of capacitance 158 F g^{-1} was attained at 3 mA cm^{-2} with the energy density of 41.2 Wh kg^{-1} along with 91% capacitance retention for over 4000 cycles [53] Zu et al. in 2014 experimented with nano-wires of $NiCo_2O_4/MnO_2$. The results depicted exceptional electrochemical characteristics of the material, additionally the asymmetric device assembled, showed that the capacitance of 112 F g^{-1} was achieved at 2 A g^{-1}. [54]. Lau et al in 2015 manufactured hierarchical $NiCo_2O_4$@NiO nanowires. The outcomes indicated the material achieved the specific capacitance of 2220 F g^{-1} and there was about 93% capacitance retention for over 3000 cycles. Additionally an asymmetric device of $NiCo_2O_4$@NiO/Activated carbon was constructed and its results depicted that energy density of about 31.5 Wh kg^{-1}

was attained and there was around 89% capacitance retention 50 A g^{-1} for over 3000 cycles [55]. Xu Y et al in 2014 synthesized porous nanowires of $CoMn_2O_4$ and $MnCo_2O_4$. The nanowires gave exceptional results, including the capacitance value of 1980 F g^{-1} at 1A g^{-1} and 1342 F g^{-1} at 1 A g^{-1} correspondingly[56]. Yan Xu in 2016 synthesized a mesoporous structure of $NiCo_2O_4$@GO has been employed as an electrode material. The specific capacitance reached around 1211.25 F g^{-1} at 1 A g^{-1}.Additionally, an asymmetric device was constructed with RGO, which gave the values of 144.45 F g^{-1} for the capacitance at 1 A g^{-1} and 51.36 W h kg^{-1} of energy density, meanwhile there was retention of capacitance was around 88% for over 2000 cycles [57]. Sahoo et al. in 2016 synthesized $ZnCo_2O_4$/RGO/NiO nano-wires. The output showed that capacitance of 1,256 F g^{-1} was attained at 3 A g^{-1} and the retention of capacitance was about 80% for over 3000 cycles. [58]. Fang et al. in 2017 worked on the material $CoMoO_4$ which had a nanoneedle morphology. The results showed the capacitance of 1628.1 C g^{-1} at 2 mA cm^{-2} and the stability of the sample was around 90% for over 5000 cycles [59]. Hu et al. in 2017 used $NiZnCo_2O_4$ to synthesize flower-like nano-wires. The output of the material exhibited the specific capacitance of around 776 F g^{-1} at 2 A g^{-1} and capacitance retention of around 91% for over 10000 cycles [60]. Wu et al in 2017 synthesized microspheres of RGO@Mn-Ni-Co oxide. The findings revealed that the value of specific capacitance reached around 646 C g^{-1} at 1 A g^{-1}. Moreover, the constructed asymmetric device of the material with N-RGO which gave the energy density of 35.6 Wh kg^{-1} and the retention of capacitance was around 77.2% for over 10000 cycles [61]. Zhao et al in 2018 synthesized $FeCo_2O_4$@GF having a hierarchal structure utilized as a positive electrode. The specific capacitance of 58.92 mF cm^{-2} was attained with 17 $\mu W \cdot h \cdot cm^{-2}$ energy density. The capacitance retention reached around 87.5% for over 8000 cycles. [62]. Heet al. in 2018 synthesized hierarchical needles of $FeCo_2O_4$@NiCo. The results showed that the material had the specific capacitance value of 2320 F g^{-1} at 1 A g^{-1}. Furthermore, its asymmetric device was assembled with activated carbon, which gave the energy density of 94.9 Wh kg^{-1} of energy density. The capacitance retention of 88.2% was achieved over 4000 cycles [63]. Fing et al. in 2019 synthesized the nano-flakes of $NiCo_2O_4$/graphene hydrogel, to be used as a positive electrode. The results showed that the energy density of 71 Wh kg^{-1} was achieved at 19.2 W kg^{-1} power density. Furthermore, rate capability of around 92% was attained for up to 5000 cycles [64].

Chapter 3

Experimentation Method

3.1 Synthesis route

synthesis of nickel cobalt oxide nanoparticles and nickel cobalt oxide@nickel cobalt selenide core/shell nanoparticles was accomplished by utilizing bottom-up approaches. Bottom-up approaches are discussed in detail below

3.2 Bottom-up approach

Chemical reactions are used to manufacture materials in bottom-up techniques. Cobalt, nickel, and zinc oxide metal nanoparticles prepared by reduction of metal salts by

- Sol-gel [66]
- Hydrothermal/ Solvothermal [67, 68]
- Coprecipitation [69]
- Microemulsion method [70]

3.2.1 Sol-gel Method

The reactants were added together to produce a solution, which is known to be hydrolysis, and later transformed into a gel, which is termed dehydration, afterwards drying using thermal treatment, in which the liquid was evaporated from the gel.

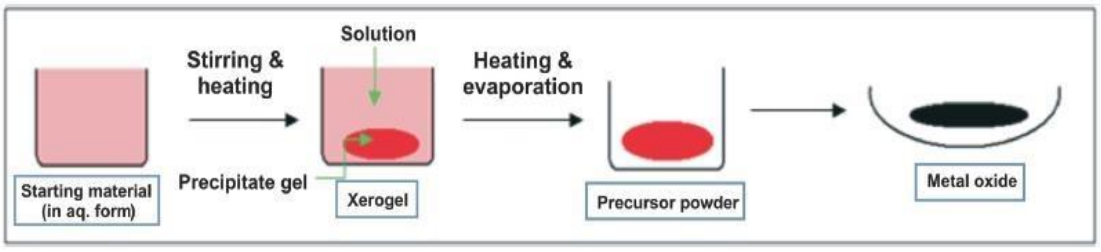

figure 3.1 Sol-gel synthesis steps

3.2.1.1 Advantages

- It is an easy and affordable method
- High purity
- Good homogeneity
- Low-temperature method

3.2.1.2 Flaws

- Weak bonding
- Difficult to regulate porosity

3.2.2 Hydrothermal/Solvothermal

A process in which the reaction occurs in presence some temperature and pressure is known as hydrothermal/solvothermal. For this procedure, a hydrothermal reactor or sealed vessel is utilized, and the precursors are distributed in the solvent and heated to a temperature over their boiling point, resulting in autogenous pressure. The process is known as hydrothermal in the case of water and solvothermal in the case of any other solvent.

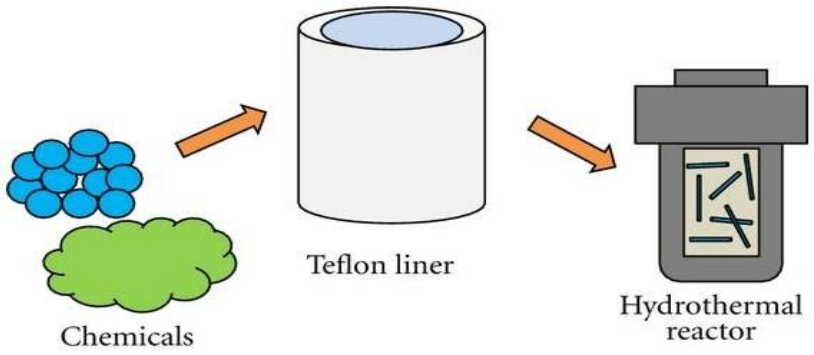

figure 3.2 Teflon lined Hydrothermal reactor

3.2.2.1 Advantages

- Simple method
- Changing time, temperature, concentration, and solvent type allows for easy and exact morphology control.

3.2.2.2 Disadvantages

- Expensive autoclaves and reactors
- Concerns about safety

3.2.3 Chemical coprecipitation

To make nanoparticles, coprecipitation is used. Precipitates are removed from the solution in this process. Contaminants are mixed into precipitates during coprecipitation. The reactant was mixed in the presence of a precipitation agent to generate a homogeneous solution, which was then dried, milled, and calcinated at a high temperature in this procedure.

3.2.3.1 Advantages

- cheap
- Eco-friendly
- Synthesis on large scale

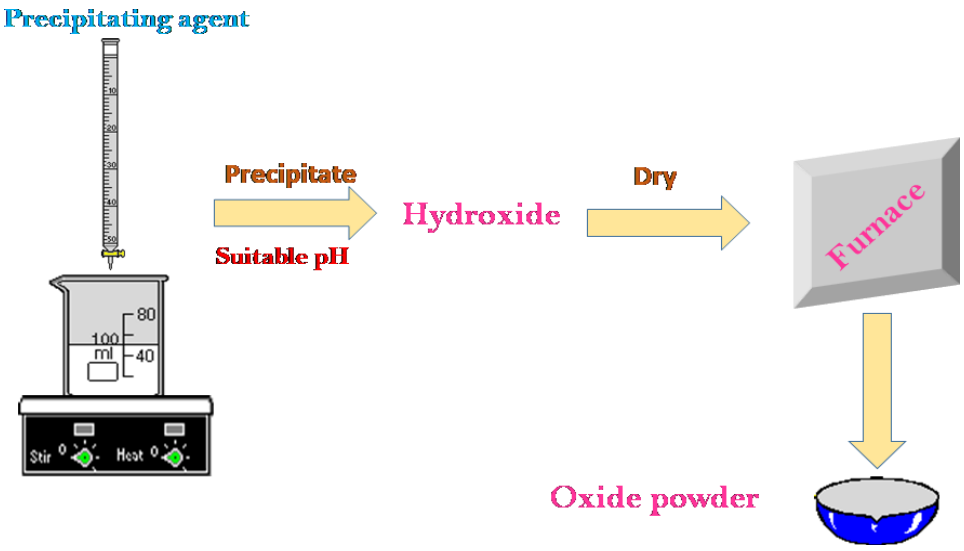

figure 3.3 Schematic of coprecipitation method

3.2.3.2 Disadvantage

Size distribution and management are extremely problematic because to poor crystallinity and agglomeration

3.2.4 Microemulsion

A microemulsion is another oxide nanoparticle production technology in which two phases are blended together and chemical reactions occur. Metal salts and surfactants make up the aqueous phase, whereas oil and water make up the other phase. Direct and reversed microemulsions were utilized, during which the oil is dispersed in water and other water is disseminated in oil, respectively.

3.2.4.1 Advantages

- It is possible to produce uniform characteristics.
- Pore size distribution is good

3.2.4.2 Disadvantage

Surfactant removal is difficult

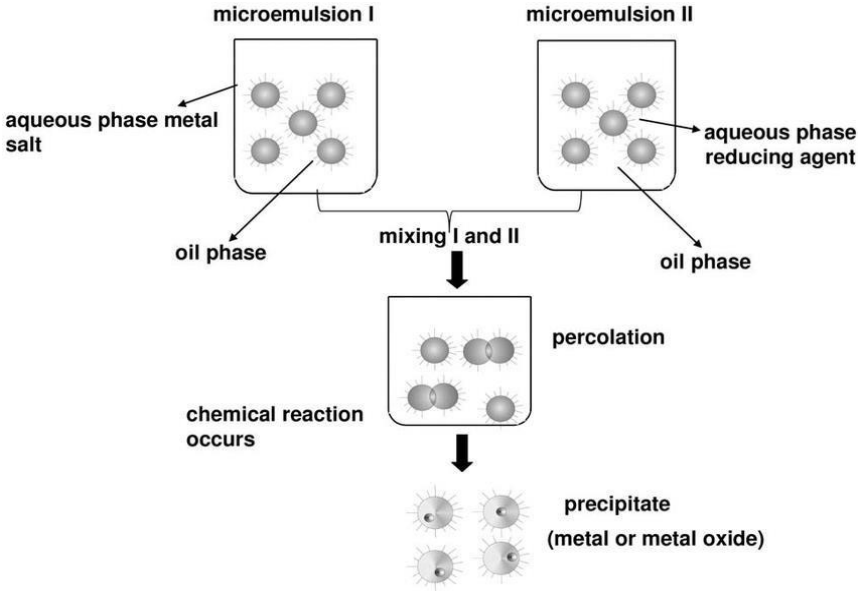

figure 3.4 Micro emulsion process

In recent times, top down and bottom-up methods are employed to manufacture

graphene sheets. Top-down methods mainly focus on exfoliation [71]

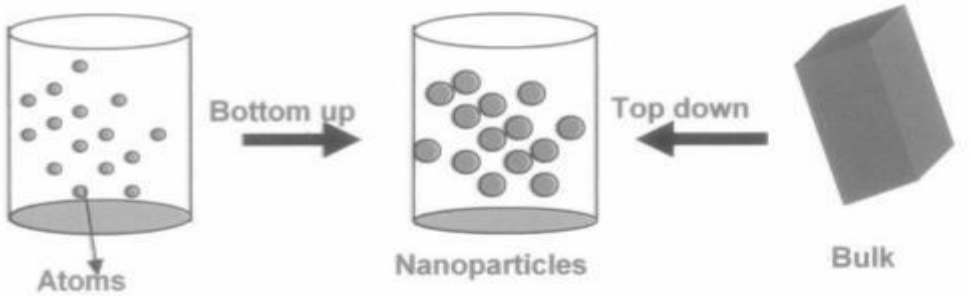

figure 3.5 Top-down and bottom-up approach schematic

3.2.5 Wet chemical synthesis

Precursors are used to prepare the target materials, and the reactions take place within the solution. Surfactants are used to manipulate the size, form, and morphology of the products that will be manufactured. Template synthesis, hydrothermal synthesis, solvothermal synthesis, self-assembly of nanocrystals, and soft colloidal synthesis are some of the most extensively utilized wet-chemical processes for nanomaterials.

3.2.5.1 Advantages

- This technology was used to successfully synthesize all 2D materials sheets and metals.
- High yield of 2D nanomaterials can be produced at a reasonable cost.
- Wet chemical techniques are better at controlling the shape of nanomaterials.

3.2.5.2 Disadvantage

- A single layer of 2D Nano sheets is difficult to achieve.

3.2.6 Chemical Vapour Deposition

CVD entails the chemical reaction of gaseous precursors at the substrate's surface in order to deposit the desired substance. Temperature, time, pressure, and yield concentration can all be used to alter the reaction kinetics.

3.2.6.1 Advantages

- Heterogeneous reactions occur, resulting in high-quality films.
- The deposition occurs quite faster.

3.2.6.2 Disadvantages

- To initiate reactions, a higher temperature is necessary.
- Chemicals and particle contamination might occur.

3.3 Top-down approaches

Exfoliation of 2D materials[72] is a hot topic for preparing mono or multi-layered materials. Exfoliated materials are significant in terms of both possible applications and fundamental research. Exfoliated graphite and TMD materials are important because they deliver a breakthrough in flexible electronics and optoelectronics devices. Strong in-plane bonding [35], [73] and weak bonding between layers in 2D materials can be isolated from each other to improve surface area and potential material characteristics. There are numerous ways to carry out this process, such as

3.3.1 Mechanical Exfoliation

The layers are separated by mechanical forces in this technique[74] he "scotch tape approach" was used to manufacture graphene from bulk graphite[72]. High-quality mono sheets can also be created using this process. This approach is popular because it creates intrinsic sheets, and it is currently the subject of a lot of research.

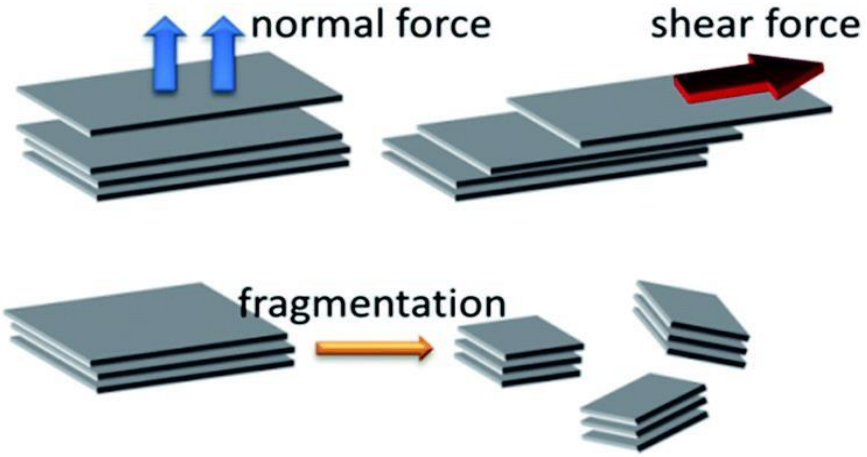

figure 3.6 Mechanical Exfoliation of 2D materials

3.3.1.1 Advantages

- In most cases, this procedure yields pristine-quality sheets.

3.3.1.2 Disadvantages

- This technique produces a low yield.
- Lack of scalability in this method[75].
- The method is only limited to small scale production.
- Controlling sheet size and thickness is a problem.

3.3.2 Liquid Phase Exfoliation

Solvents are utilized to intercalate the layers of chemical in this process. Solvents are utilized that have a similar surface energy to that of the layered material's crystal lattice. When an appropriate solvent in used in the mixture, sonication forms nanosheets that are stabilized[76]. To achieve well-defined structures, certain surfactants may be applied. For the preparation of mono- and few-layered structures from bulk, sonication assisted exfoliation is currently widely employed. Sound energy is used in sonication, resulting in shear forces. Cavitation bubbles are formed, and as they collapse, the layers are peeled away.

The solvent is an important consideration since it must aid in the delimitation process. It should be able to maintain highly stabilized dispersions with a high concentration of 2D exfoliated sheets for an extended period of time. For efficient exfoliation of materials, a mixture of solvents is sometimes used. NMP is the most prevalent solvent. The surface energy of NMP is 40 mJ m-2, which is similar to that of many-layered materials[77]. n NMP, stable graphite dispersions of up to 40 mg ml-1 having surface energy 75 mJ m-2 could be achieved.

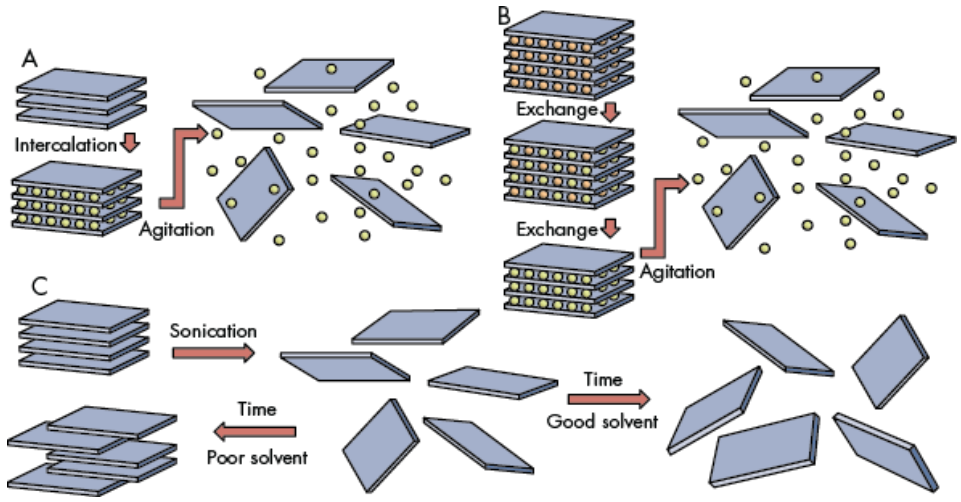

figure 3.7 Liquid phase exfoliation of 2D materials

3.3.2.1 Advantages

- This method produces a high yield. This method is not air sensitive.
- There are no chemical reactions
- The result is a very crystalline product.
- This procedure is extremely straightforward and cost-effective.
- Good scalability sheets are obtained.

3.3.2.2 Disadvantages

- The Remaining chemicals in solution-based exfoliation may alter the characteristics of Nano sheets such as graphene. The solvent used could be volatile or toxic.

- This approach can create faults in two-dimensional materials and decrease the flake size to a few hundred nanometers.

3.4 Aim and Objectives

This study aims to synthesize a porous material for supercapacitor application. This study includes

- Synthesis of Nickel cobalt oxide via hydrothermal method
- Synthesis of nickel cobalt oxide @Nickel cobalt selenide core/shell via wet chemical method.
- Employing nickel cobalt oxide as an electrode in a supercapacitor
- Electrochemical performance testing of prepared materials.
- Asymmetric supercapacitor testing by employing nickel cobalt oxide as positive and Activated carbon as a negative electrode material.
- Furthermore, such materials could be employed for other energy storage appliances like batteries.

3.5 Selected Synthesis Method

The hydrothermal method is adopted for the manufacturing of metals oxide Nano particles because of control in the morphology and structure i-e nanorods, nanoflowers, nanowires can be attained by varying temperature and time of the reaction.

3.6 Materials Required

- Cobalt Nitrate Hexahydrate
- Nickel Nitrate Hexahydrate pure
- Urea $CO(NH_2)_2$>98%
- Ammonium Flouride NH_4F
- Potassium Hydroxide KOH

- Nafion@deflourinated resin solution
- Ethanol
- Distilled Water
- Pure Selenium powder from Sigma Aldrich.
- Sodium Borohydride $NaBH_4$ was purchased from DAEJUNG

3.7 Apparatus used

Apparatus used for the synthesis of oxide and selenide

- Teflon lined stainless steel autoclave
- Oven
- Magnetic stirrer
- Hotplate
- Beakers
- Petri dishes
- Weighing balance
- Fume hood
- Vacuum filtration
- Filter papers
- Muffle Furnace

3.8 Synthesis of Nickel Cobalt Oxide (NCO)

In the first step, 50 ml of distilled water was taken in a beaker then 0.3 M Nickel nitrate hexahydrate, 0.6 M Cobalt nitrate hexahydrate, 1.2 M Urea, and 0.4 M Ammonium fluoride were added and magnetically stirred for 2 hours. The uniform mixture was then poured into an 100ml autoclave having a Teflon lining. The autoclave was placed in the oven for five hours at 130 degrees Celsius. The precipitates were then washed multiple times with distilled water before being vacuum filtered to remove the absolute ethanol and precipitates. The sample was then dried at 60°C for 6 hours before being

annealed at 350°C at 2°C/min in a muffle furnace for 2 hours to yield the NCO.

3.9 Synthesis of NCO@Nickel Cobalt Selenide (NCSe) core/shell

In 30 ml of water, 0.2 mmol Se and 1.2 mmol NaBH4 were dissolved to make a Se2 source solution. By immersing the NCO nanowires within the above-mentioned source solution alongside maintaining their temperature at 50°C for the time of five hours, hierarchical Mesoporous nanowires of NCO/NCSe core/shell were synthesized. Following that, samples were cleaned using 100% ethanol and deionized water before being dried in a nitrogen blower.

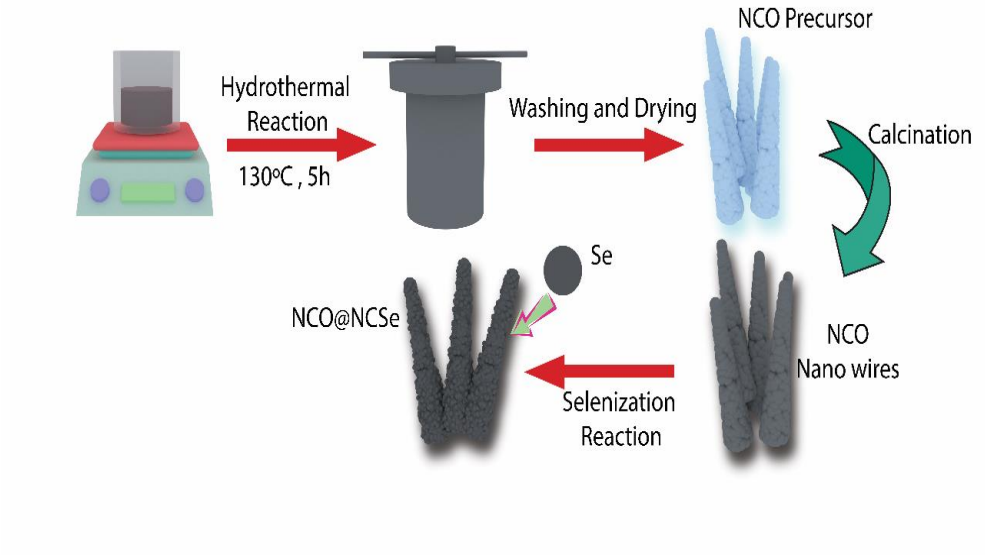

figure 3. 8 Synthesis route of NCO//NCSe

Chapter 4

Characterization Techniques

4.1 Scanning Electron Microscope

In this technique, fine beam of electrons is focused over a specimen's surface. Photons or electrons are knocked off from the material's surface in the result. These knocked off electrons are then focused on the indicator. The luminance of the cathode ray tube (CRT) is regulated by the detector's output. Every time the beams come into contact, a consequent point on CRT is plotted and the material's image is produced [78].

The electron-surface interaction causes the release of secondary electrons (SE), backscattered electrons (BSE) and X-rays [79]. Common SEM mode for detection is via secondary electrons. These electrons are emitted from near the sample surface. So, a pronounced and clear image of the sample is obtained. It can reveal sample detail even less than 1nm in size. Also, elastic scattering of incident electrons also takes place and release back scattered electrons. They emerge from deeper locations as compared to secondary electrons. So, their resolution is comparatively low. When an inner shell electron knocks off from its shell it emits characteristic x-rays [80].

We use SEM as it has easy sample preparation, and we can figure our sample's morphology, chemistry, crystallography, and orientation of planes. Magnification of SEM can be controlled from 10 to 500,000 times.

Morphology of the materials were examined on (JEOL-JSM- 6490LA) and FESEM analysis were performed on (MIRA3 TESCAN). Elemental composition was determined by EDS detector attached to FESEM.

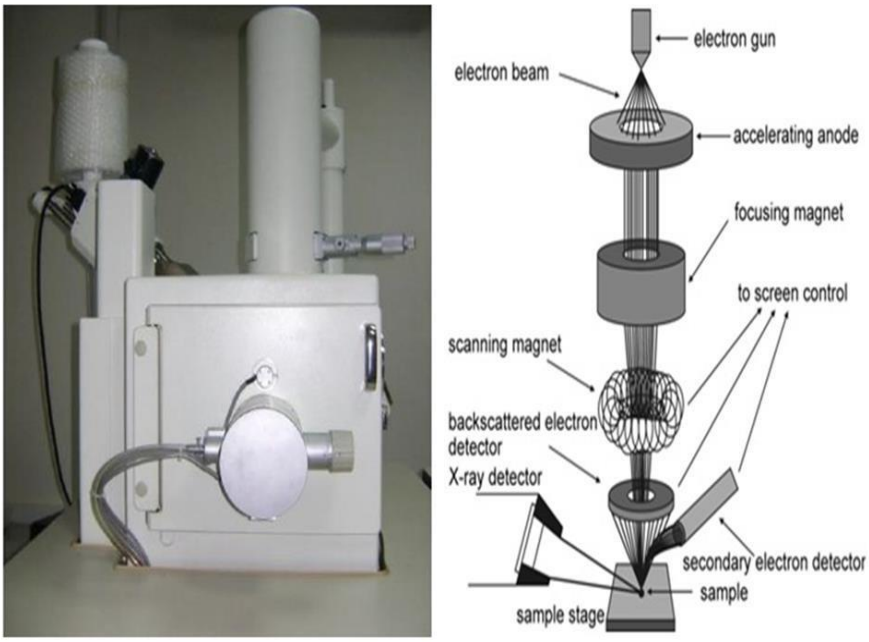

figure 4.1 (a) JOEL JSM-6490LA present at SCME; (b) SEM Schematic

4.2 X-Ray Diffraction (XRD)

For determining the crystal assembly of the material this technique is employed. It is a non-destructive technique, and it provides fingerprints of Bragg's reflections of crystalline materials. It consists of 3 main parts. A cathode tube, sample holder and detector. X-rays are produced by heating filament element which accelerates electrons towards a target which collide with target material with electrons. Crystal is composed of layers and planes. So, x-ray which has wavelength having similar to these planes is reflected that that angle of incidence is equal to the angle of reflection. "Diffraction" takes place, and it can be described as by Bragg's Law:

$$2d\sin\theta = n\lambda \quad (4)$$

When Bragg's law is satisfies, it means there is constructive interference, and "Bragg's reflections" will be picked up by the detector. These reflections positions tell us about inter-layer spacing-ray diffraction tells us about the phase, crystallinity, and sample purity. By this technique, one can also determine lattice mismatch, dislocations, and unit cell dimensions.

X-ray diffractions were performed by STOE diffractometer at SCME-NUST. The scan angle was taken in

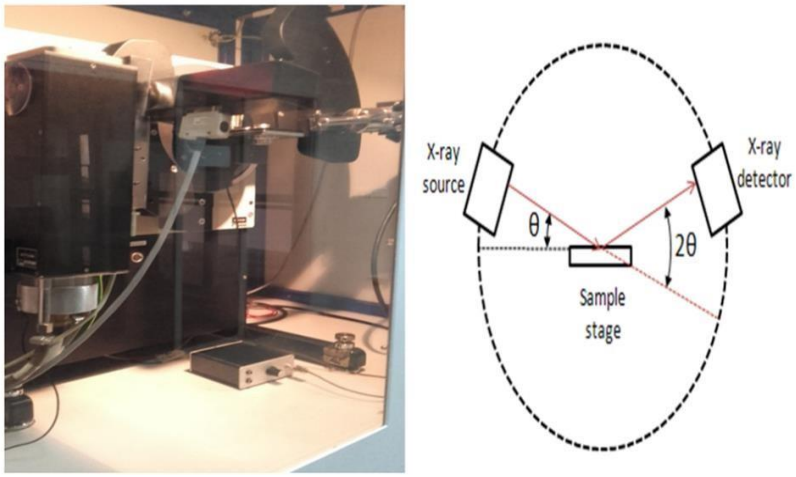

figure 4.2 XRD present at SCME- NUST (b) XRD basic schematic

4.3 Brunauer Emmett Teller (BET)

Surface area and porosity are among the vital property of a material which can be determined by BET analysis technique[81]. Equipment consists of several parts, sample preparation device, vacuum system, sample tube/dewar, N_2 transfer system, computer hardware, and software Working principle of BET is sample drying at elevated temperature with the purging of non-corrosive gases like N_2 then the amount of adsorbing N_2 is related to the specific surface area along with pore volume. Sample preparation is a key step for BET analysis. First, the calculated amount of sample is purified by degassing to remove the extra atmospheric contaminants like water vapors and air under elevated temperature for the desired amount of time under vacuum conditions in the sample preparation device. Then the sample test tube was placed in the surface area, and porosity analysis which relates to the computing system and amount of adsorbing gases is calculated, related to the surface area and overall pore volume. BET analysis was performed at Gemini® VII 2390 instrument is present in SCME the advantage of this equipment is accurate, fast and simple to operate.

Operating conditions were degassing of the sample at 300°C for 3 hrs. and analysis were performed at 0.05 to 0.3 p/p^0 range

figure 4.3 Gemini® VII 2390 Micro porosity analyser

4.4 Electrochemical Workstation:

Biologic VSP is the research-grade potentiostat present at SCME. Equipment consists of workstation, electrochemical cell, computer hardware, and software system. It is used for many applications including

- Battery testing
- Fuel cell and biofuel cell
- Liquid conductivity
- Electrochemical deposition of thin film
- Material impedance spectroscopy,
- Corrosion testing
- Photovoltaics and sensors
- Capacitor and supercapacitor testing

Supercapacitor testing was performed on this potentiostat such as,

- Cyclic voltammetry (CV)
- Galvanostatic Charge-Discharge (GCD)
- Electrochemical Impedance Spectroscopy (EIS)

figure 4.4 Biologic VSP Electrochemical Workstation

4.4.1 Cyclic Voltammetry (CV)

It is the simplest technique in laboratory scale to measure the electrochemical behavior. Oxidation and reduction which occurs at the interface of the electrode/electrolyte can be analyzed by CV. CV system consists working electrode (WE), a reference electrode (RE), and the counter electrode (CE). In CV, the potential is charged on the WE and RE and resulting output current response is recorded between the working and counter electrode. CV curve is the resulting current(I) of WE vs. the potential (V). Potential is applied between the WE and the RE. For the RE, usually the saturated calomel electrode (SCE) and Silver/Silver chloride (Ag/AgCl) are used. The counter electrode is mostly Platinum. The purpose of the electrolyte is to provide ions. Electrolyte must possess good conductivity. In supercapacitors, different materials show different responses. EDLC gives rectangular curve whereas pseudo capacitor gives oxidation and reduction hump during forward and reverse scan.

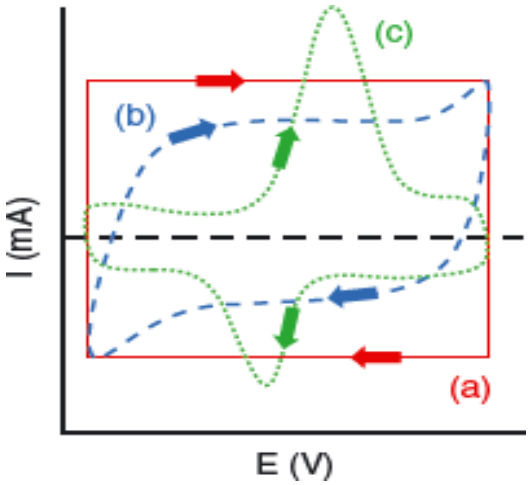

figure 4.5 CV plot of (a) Ideal capacitor with perfect rectangular shape (b)EDLC material with near rectangular shape(c)Pseudo capacitor with oxidation and reduction peaks [10]

4.4.2 Galvanostatic Charge-Discharge (GCD)

GCD is the most common method to test the charging and discharging of the supercapacitors as well as batteries. In GCD measure the potential with time at constant current. One charge and discharge of the material is equal to one complete cycle. Similar to CV, GCD curves of EDLC and Pseudo capacitor is different. EDLC materials In EDLC type supercapacitors the charge-discharge cycles show linear curves with very little IR drop whereas in case of Pseudo capacitors the curve is not linear and IR drop is large in comparison with the EDLC. This deviation refers to the charge storage mechanism which take place due to the oxidation and reduction reactions. Similarly, the linear response shows that charge storage mechanism is not faradaic means that only physical charge storage occurs.GCD curves of both EDLC and Psuedocapacitor in Figure 4.6.

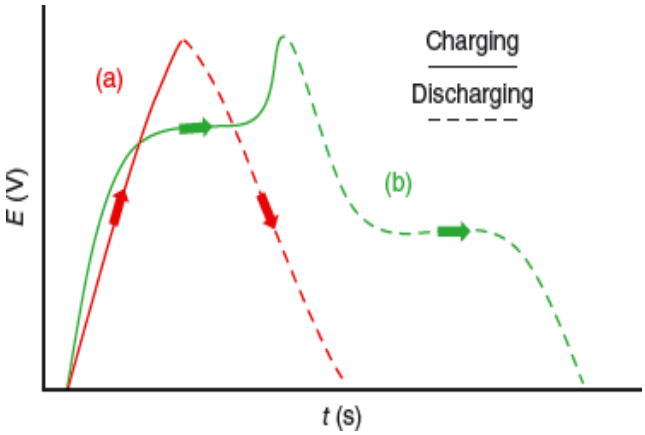

figure 4.6 GCD curves of (a) EDLC (b)Pseudo capacitor [10]

4.4.3 Cyclic Stability

Cyclic stability is an essential parameter for the energy storage devices. Cyclic performance of supercapacitors is tested by multiple charge-discharge cycles. On lab scale normally 500 to 10000 charge-discharge cycles were conducted to examine the capacitance retention of the material.

4.4.4 Electrochemical Impedance Spectroscopy (EIS)

EIS is utilized to measure the dielectric characteristics of a material as a function of frequency. It measures impedance of the material. The Nyquist plot is plotted to base on the equivalent circuit as a response of the system. It is the impedance of a frequency. For Supercapacitor application

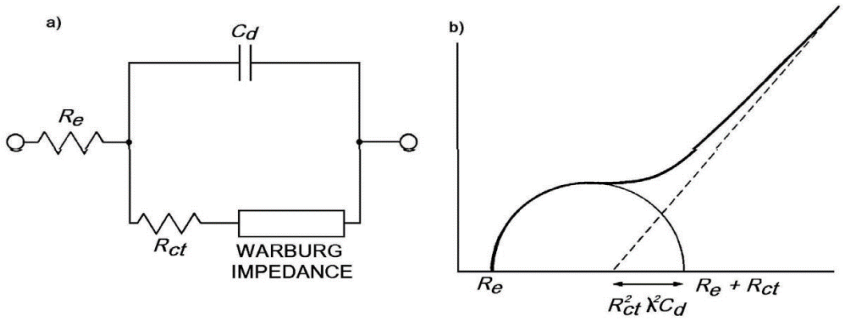

figure 4.7 EIS (a) Equivalent circuit diagram (b)Nyquist plot

Here Re is resistance which is series resistance at working electrode-electrolyte interface, Rct is charge transfer resistance or polarization resistance, Cd is the double layer capacitance defined as interface capacitance which is between electrode and electrolyte and warburg impedance which depends on diffusion of reactants.

Chapter 5

Results and Discussions

XRD assessment was accomplished to ascertain the crystal structure of prepared materials. Most of the peaks matched to JCPDS card no 01-073-1702 (Nickel Cobalt Oxide) peaks corresponding to angle 18.8, 31 ,36, 38, 44, 56,59 ,64 and 77 belongs to (111), (220), (311), (222), (400), (422), (511), (440), (533) respectively. Its crystal structure is cubic and space group is Fd-3m. The remaining 2 peaks matched to JCPDS card no 00-020-0335 (Nickel Cobalt Selenide) peaks corresponding to angle 29.7 and 39.5 belongs to (202) and (301) respectively. Its crystal structure is tetragonal and space group is I-4m2.

The crystallite size of NiCoSe was assessed through

$D = 0.9\lambda/(\beta \cos \theta)$ …… *(5)*

Where θ is the angle of the diffracted peak, B is FWHM, λ wavelength. The average crystallite size of NiCoSe is 33.7 nm

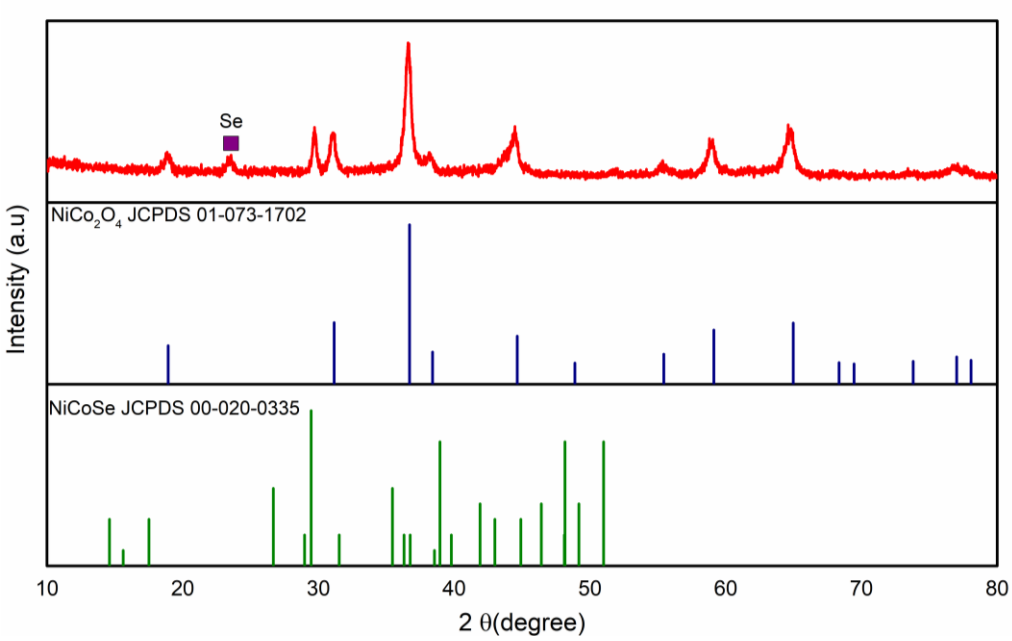

figure 5.1 XRD analysis of NCO//NCSe

To examine the morphology of nickel cobalt oxide (NCO) SEM analysis was carried out. NCO exhibit hierarchical mesoporous nanostructure. The nanowires are arranged in one dimension hierarchically. one thorn ball is of 3 µm to 5µm in which nanowires were arranged. Nanowires are arranged in one direction which affirmed the porous nature of the material as well as good transport of electrolyte during an electrochemical performance.

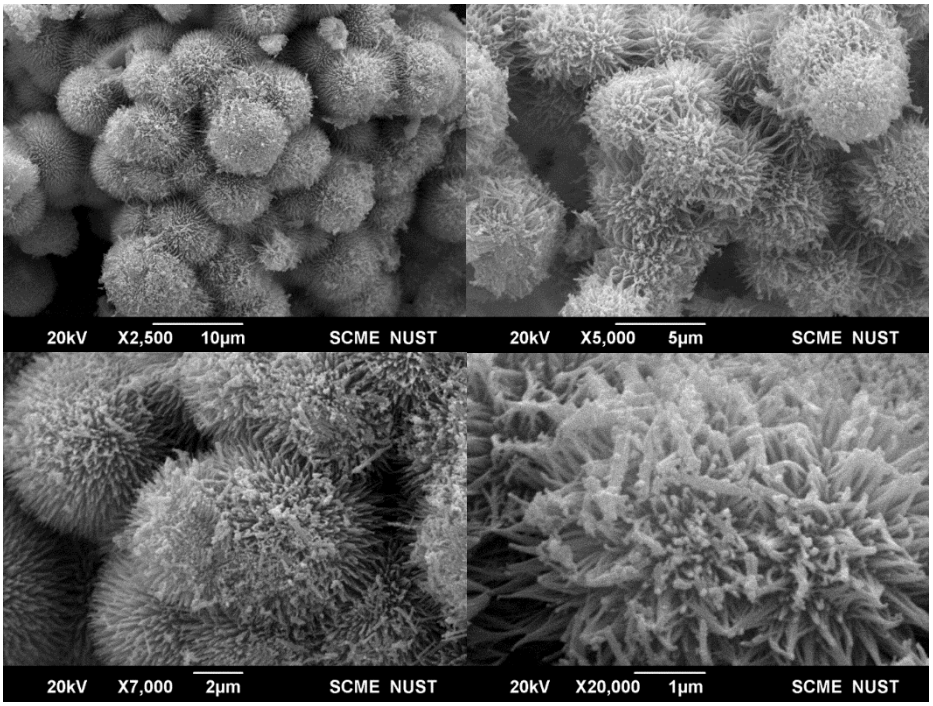

figure 5.2 Scanning electron microscopy of Hierarchical NCO nanowire at low and high magnification

Nickel Cobalt oxide@Nickel cobalt Selenide core/shell morphology was examined by SEM. The SEM analysis of NCO/NCSe shows the hierarchical nanostructures. Nanowires are arranged in one direction which affirmed the porous nature of the material as well as good transport of electrolyte during an electrochemical performance. Mesoporous flower-like structure is clearly shown in Figure 2c. The mesoporous structure provides large specific surface area which can accommodate numerous electrolyte ions to participate in faradaic reaction. The volume expansion that occurs during reversible cycling are accommodated by the open spaces present between the nanowires which results in superior cyclic performance of the material. The pores in the structure also store electroactive species which are used in faradaic

redox reactions. The further analyses of the materials revealed that the nanowires are interconnected. This morphological interconnection at nanoscale enhances the surface area and enables the fast mass diffusion at higher current densities. The aforementioned properties will endorse the high-rate capability of the synthesized material. Additionally, volume changes that occur during reversible cycling are accommodated by the open spaces present between the nanowires which results in superior cyclic stability of the material.

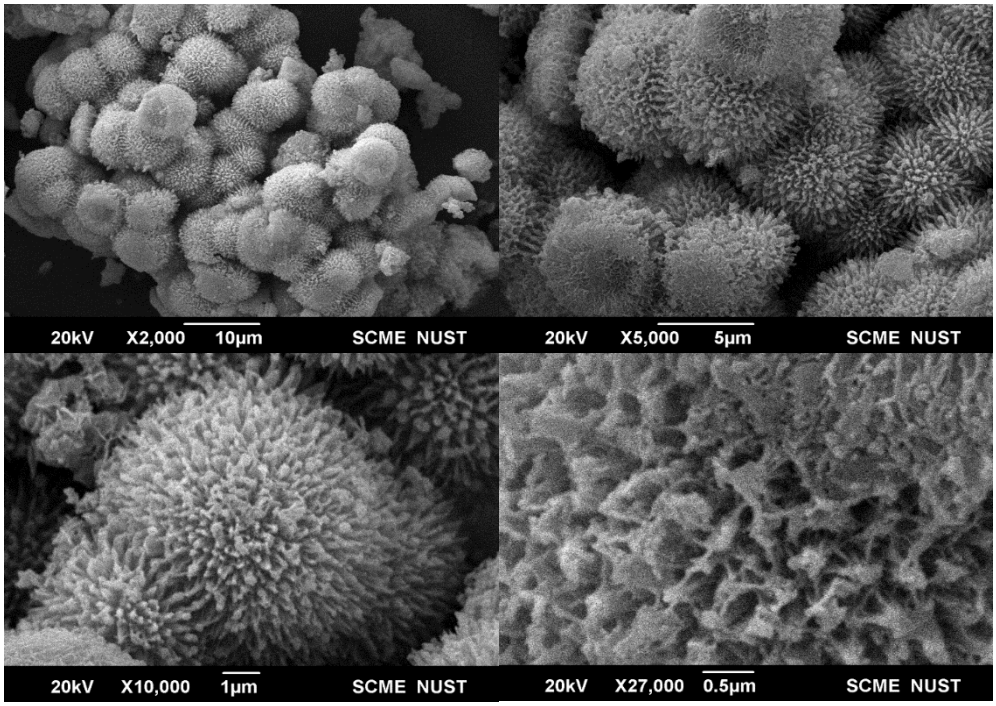

figure 5.3 Scanning electron microscopy of Hierarchical NCO//NCSe nanowire at low and high magnification

Elemental analysis of NiCoSe was performed by the EDS detector attached to the SEM.EDS analysis confirmed the desired elements Nickel, Cobalt, selenium and Oxygen of 15.6,30.4,8.8 and 45.1 atomic weight percent, respectively. EDS analysis affirmed that Cobalt cations were replaced by nickel and selenium cations which limits the high resistivity problem of the cobalt oxide as the ions transport mechanism was enhanced by the replacement of cations

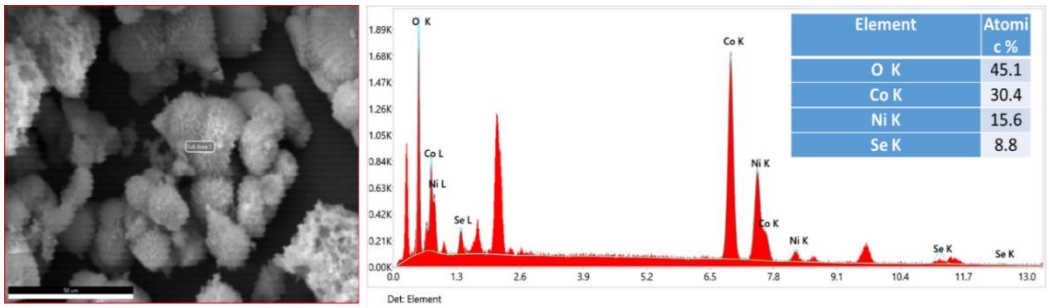

figure 5. 4 Elemental analysis of NCO//NCSe

Elemental mapping of NiCoSe was performed by the EDS detector attached to the SEM. The mapping shows homogeneous distribution of Nickel, Cobalt, Oxygen and Selenium. We can see no stray selenium in the sample which indicates the complete selenization of the sample.

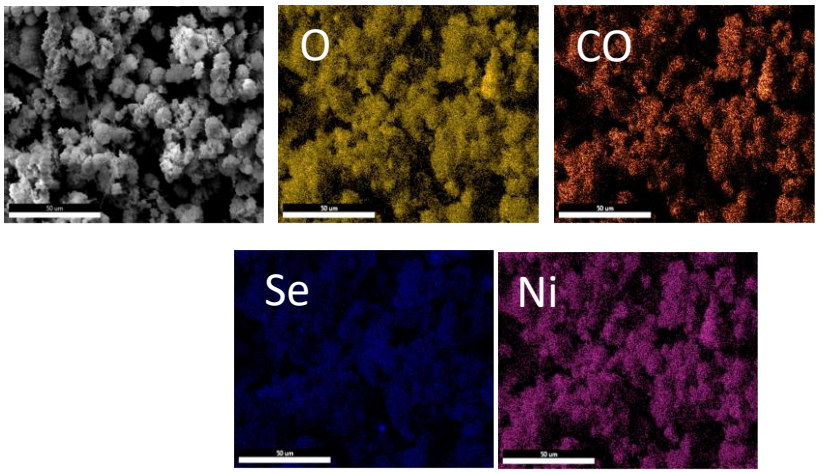

figure 5.5 Elemental mapping of NCO//NCSe

To evaluate the specific surface of the produced samples, a nitrogen absorption test was conducted. Surface area and porosity has a linear relationship with the electrochemical performance. BET specific surface area of NCO/NCSe mesoporous nanowires is 55.11 m^2/g with pore volume of 0.1811 cm/g^3 while the surface area of NCO is 51.39 m^2/g with pore volume of 0.083 cm/g^3. Because NCO/NCSe has a large specific area, it efficiently transfers electrolytes across the electrode material, increases the number of active sites which results in greater electrochemical functioning. The Nitrogen absorption isotherms samples are displayed in Figure 5.6.

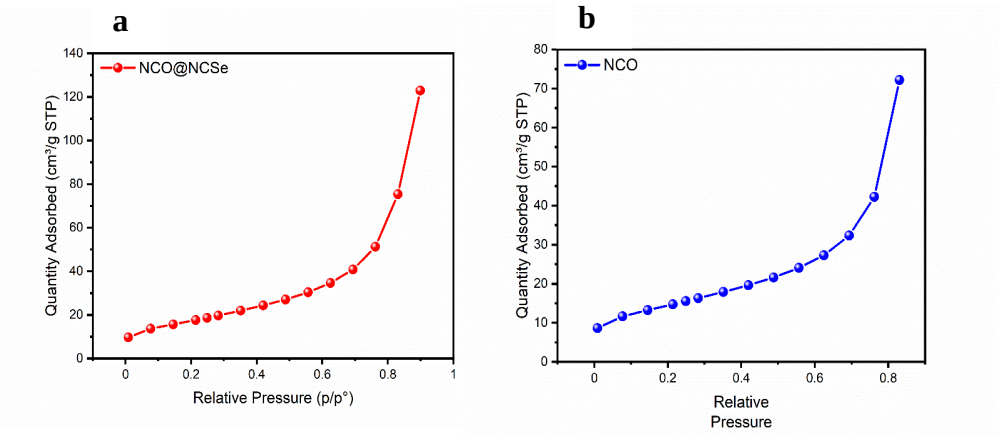

figure 5.6 N_2 absorption isotherm (a) NCO//NCSe (b) NCO

Using a Biologic VSP electrochemical workstation, all electrochemical assays were performed alongside each other at room temperature. The working electrode was prepared using the conventional slurry-coating technique. Initially, ethanol was used to combine the active ingredients, NCSe and nafion, and then the mixture was sonicated for 1 hour to form slurry. Following the preparation of 1 cm2 of foam nickels, the slurry was pasted into the Ni foam, and the electrode was dried under vacuum before being pressed at 10 MPa. Ni foam was weighed before and after the electroactive material was loaded in order to calculate the mass loading of the substance. To perform the electrochemical test, the electrode employed was of a relatively higher mass, in which the mass of electroactive material ranged between 1-2mg. Utilizing a three-electrode configuration with 6 mol of KOH solution as the electrolyte and a piece of Pt wire as the counter electrode, the performance of the electrode's ability to store charge was examined. The synthesized samples, Ag/AgCl and Pt electrodes are used as working electrodes, reference electrodes and counter electrodes, respectively. The CV, GCD and EIS tests measured the charge storage performance. The following equation was used to determine an electrode's specific capacitance from the GCD curves.

$$Cs = \frac{I*t}{m*\Delta V} \quad \ldots\ldots\ldots\ldots (7)$$

Here, “t” is discharge time, “I” represents current density and “m” is mass of active material, ΔV is the voltage drop during discharge.

Cyclic Voltammetry was conducted to establish the faradaic response of NiCoO and NiCoSe at different scan rates in the range of 5 mV s^{-1} to 100 mV s^{-1} with a potential window of 0 V to 0.5 V. The nonrectangular shape as shown in Figure 5.15 confirms the faradaic redox reaction and the pseudocapacitive nature of NiCoO and NiCoSe electrode material. Redox peaks were examined in the CV curves of NiCoO and NiCoSe The peak position of samples was at different ranges which represents the unconventional materials having different polarization. Increasing the scan rate peaks were shifted from its position shows the different polarization and redox reaction is limited results in less prominent peaks. Transition Metal Selenide nanowires NiCoSe shows the highest specific capacitance as compared to binary oxide. NiCoSe have greater integrated area as compared to the NiCoO due to the replacement of Cobalt cations with the Selenide cations which results in the better electrochemical performance as well as the specific capacitance. With the increase in the scan rate, the specific capacitance decreases as there would be limited faradaic redox reaction as the availability of the active sites would be lesser in comparison to the lowest scan rate at which the capacitance would be high because of the presence of more redox active sites. The specific capacitance of NiCoSe and NiCoO was calculated at different scan rates by using

$$Cs = \frac{\int idV}{(Vs * m * \Delta V)} \ldots\ldots\ldots\ldots (6)$$

Here Cs represents specific capacitance, $\int i dv$ is the integrated scan area, Vs represents scan rate, m is the active mass which was 0.01 mg and ΔV is the operating potential window.

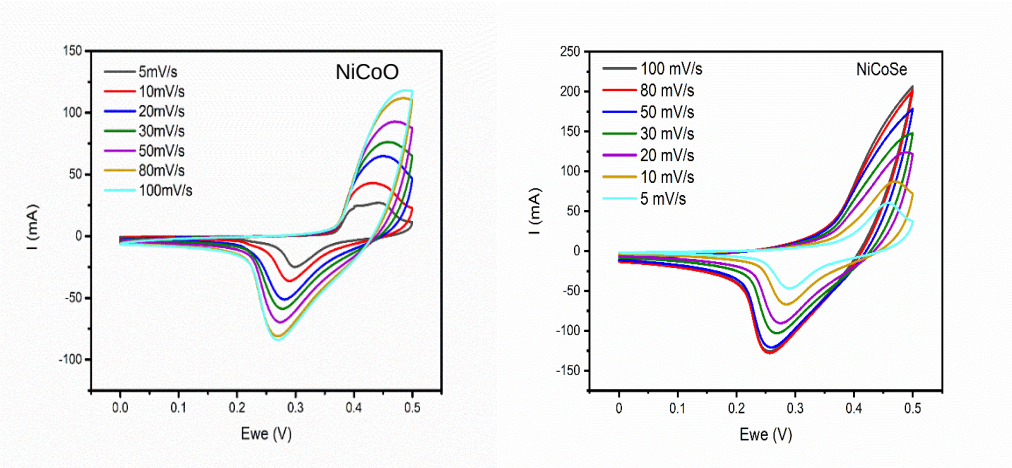

figure 5.7 CV curves at different scan rates (a) NCO (b) NCO//NCSe

on workstation at different current densities and capacitive performance was analyzed further. Figure 5.8 shows

GCD curves of NCO and NCSe from the range of 1 A g^{-1} to 10 A g^{-1} with operating window of 0V to 0.5 V. Faradaic behaviour of all the different materials reveals from the GCD curves as all the curves of materials shows nonlinear response which shows the faradaic reaction occurs and charge storage mechanism is due to oxidation and reduction. It is evident from the curves that NiCoSe exhibits longer discharge time in comparison with other binary metal oxide (NiCoO), demonstrate that the electrochemical performance of NiCoSe was far superior due to replacement of cobalt cations with Selenide cations. Also, NiCoSe shows more discharge time as compared to binary metal oxide (NiCoO).

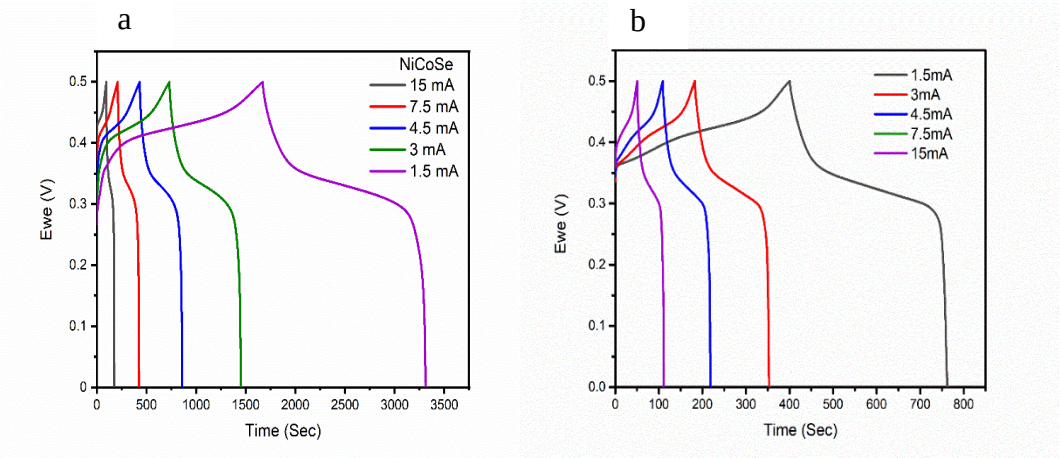

figure 5.8 GCD curves of (a) NCO//NCSe (b) NCO

GCD is the most accurate way to calculate specific capacitance. Specific capacitance is calculated by

$$Cs = \frac{I*t}{m*\Delta V} \ldots\ldots\ldots\ldots (7)$$

Here, "t" is discharge time, "I" exhibits current density and "m" is mass of active material, ΔV is the voltage drop during discharge.NiCoSe shows good specific capacitance of 3281.544 F g^{-1}, 2876.18 F g^{-1}, 2570.5 F g^{-1}, 2154.96 F g^{-1} and 1611.36 F g^{-1} at 1 A g^{-1}, 2 A g^{-1}, 3 A g^{-1},5 A g-1 and 10 A g-1 as shown in Fig 5.8 .Moreover NiCoO exhibits less performance as compared to NiCoSe as NiCoO shows Capacitance of 773 F g^{-1}, 728 F g^{-1}, 700 F g^{-1}, 658 F g^{-1}, and 580 F g^{-1} at at 1 A g^{-1}, 2 A g^{-1}, 3 A g^{-1},5 A g^{-1} and 10 A g^{-1} and Table 4. Energy density and power density was calculated by

$$\text{Energy Density (ED)} = \frac{1}{2} Cs\Delta V \ldots\ldots\ldots\ldots (8)$$

$$\text{Power Density (PD)} = \frac{ED}{\Delta t} \ldots\ldots\ldots\ldots (9)$$

Here, Cs is the specific capacitance calculated from CV or GCD and ΔV is the operating voltage, and Δt is discharge time.

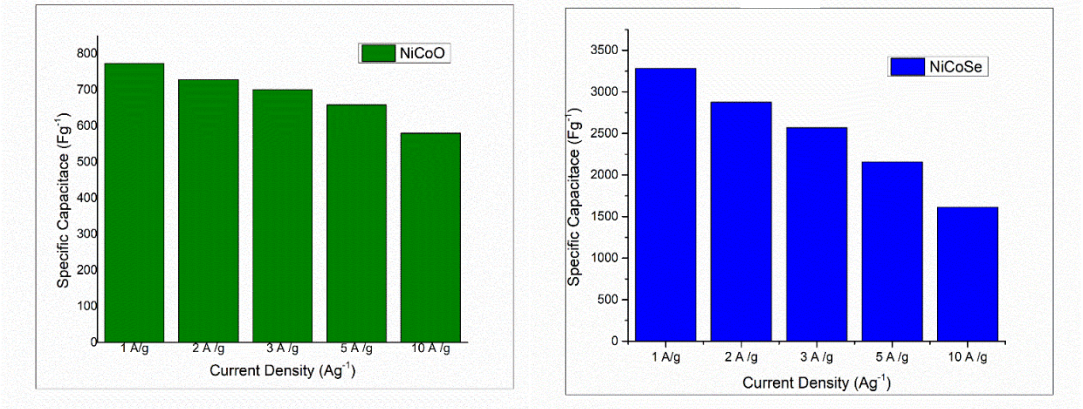

figure 5.9 Specific Capacitance at different current densities (a) NCO (b) NCO//NCSe

The assembly of asymmetric super capacitor was accomplished by combining NCO/NCSe and activated carbon as positive and negative electrodes respectively. NCO/NCSe NWs and Nafion solution were added to the ethanol in an 85:5:10 ratios, then ultrasonic homogenization was performed for 60 minutes. The above suspension was gradually dropped over conducting electrode after desiccating it in vacuum oven for 1 hour to make positive electrode. Activated carbon and Nafion solution were added to the ethanol in an 85:5:10 ratios, followed by ultrasonic homogenization for 60 minutes. The aforementioned suspension was slowly dropped over conducting electrode followed by drying in vacuum oven for 60 minutes to make the negative electrode. For the tests, a voltage window of 0 V to 1.5 V was selected. The balancing of charge within the positive and negative electrodes strongly influenced the asymmetric SC performance. For the determination of mass loading on electrode, the following expression was used

$$\frac{m^+}{m^-} = \frac{c^- \times \Delta v^-}{c^+ \times \Delta v^+}$$

Where m is the mass (g) of the electrodes. C is the specific capacitance (F g^{-1}), and 1.5V is the potential window. Optimized mass to charge ratio is 0.5.

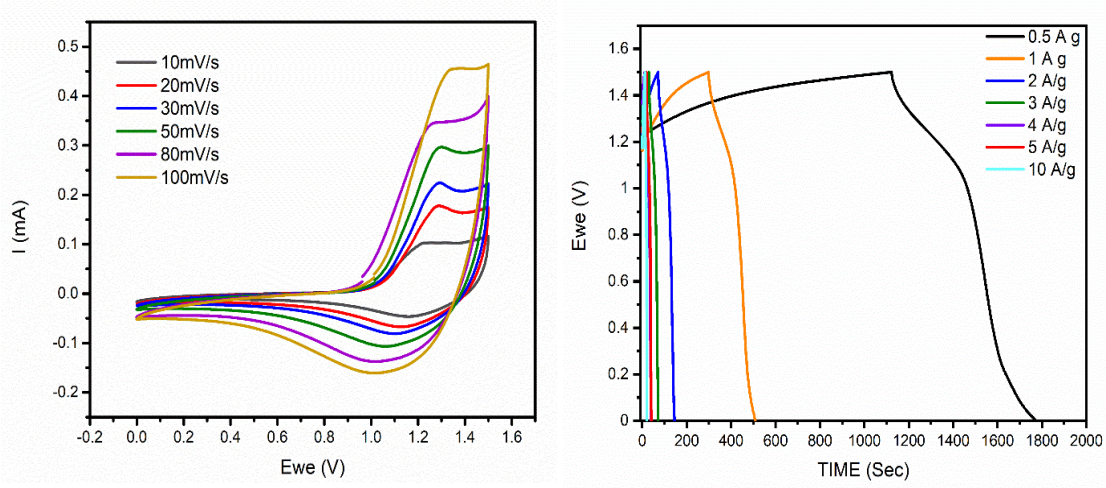

figure 5.10 CV and GCD curve of NCO//NCSe at different scan rates

The Device was tested at voltage window of 0V to 1.5 V. All the CV bends lies between 10 mV s^{-1} to 10 mV $s^{-1}$and GCD bends from 0.5 A g^{-1} to 10 A g^{-1} current densities were shown in Figure 5.10. CV curves are shown in Figure 5.10(a) which remain almost the same from low to high scan rate demonstrate the excellent capacitive behavior of the device. GCD curves at various

current densities varying from 1 A g^{-1} to 10 A g^{-1} are shown in the Figure 5.10(b). Curves show the pseudocapacitive behavior both from CV as well as GCD.ASC shows high specific capacitance of 121.33 F g^{-1} at 1 A g^{-1} and 71.66 at 5A g^{-1} current densities. Specific capacitance estimates at different current densities were given in Table 5.1

table 5.1 Specific Capacitance and different current densities

Current Density (A g^{-1})	Specific Capacitance (F g^{-1})
1	121.33
2	98.66
3	84
4	78.68
5	71.66
10	56.66

ASC exhibits high energy density of 37.91 Wh kg^{-1} at a power density of 749.95W kg^{-1} as seen in Ragone plot in Figure 5.11. Energy density and power density was calculated by

$$\text{Energy Density (ED)} = \frac{1}{2} Cs\Delta V \text{ ……. (8)}$$

$$\text{Power Density (PD)} = \frac{ED}{\Delta t} \text{ ……. (9)}$$

Here, Cs is the specific capacitance calculated from CV or GCD and ΔV is the operating voltage, and Δt is discharge time.

From the results a high value of energy density was achieved with higher power densities, which can be credited to NCSe NWs as they had a porous structure, due to which there is a larger electrode/electrolyte interface and hence a faster mass transport at higher current densities.

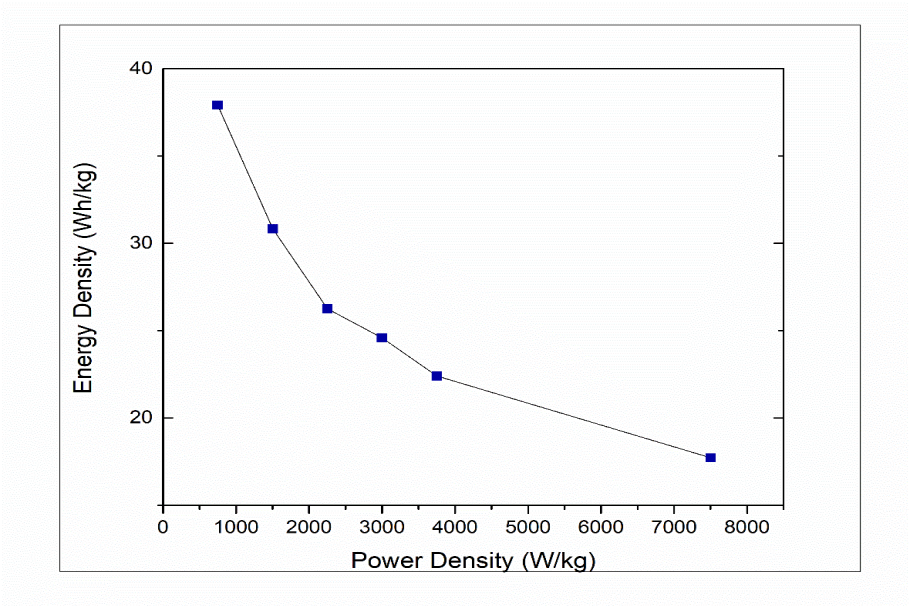

figure 5.11 Ragone plot of asymmetric device

EIS was used to analyse the solution resistance (Rs) and charge transfer resistance (Rct). The Nyquist plot is made up of a semicircle and a straight line, where the diameter of the semicircle stands in for the Rct, which is essentially a measurement of the difficulty involved in shifting an electron from one atom or compound to another. It resembles other types of electrical resistance quite a bit. The amount of energy lost during the charge transfer increases with Rct measurement value. NCSe nanowires show low Rct value of 5.525 Ohm which means that electrons have to face less resistance which results in excellent electrochemical performance of material. EIS was performed after the stability of 7000 cycles and there is small increase in Rct value as it reaches to 9.587. The minimum increase in the Rct value can be linked to the minimal deterioration in the structure of nano wires due to cyclic loading. Minimum Rs, and Rct value of NCSe affirmed the excellent material for supercapacitor. The Nyquist plot is shown in Figure 5.11, Table shows the Rct values of NCSe.

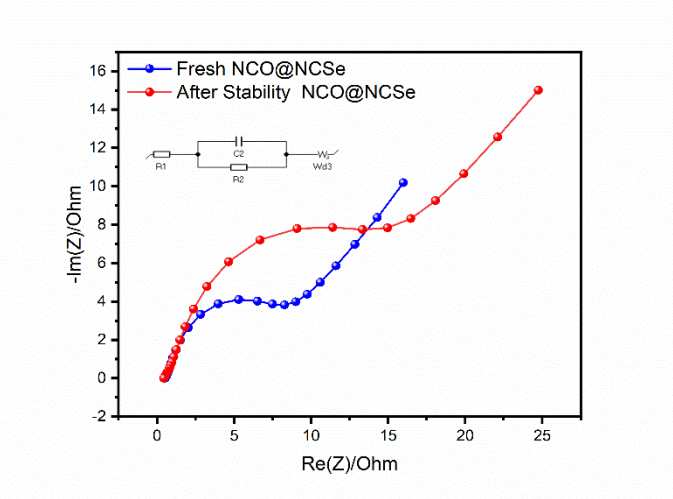

Sample	Rs (ohm)	Rct(ohm)
NCO//NCSe	0.5225	5.525
NCO//NCSe after stability	0.441	9.587

figure 5.12 Nyquist plot of NCO//NCSe before and after 7000 cycles stability

The cyclic stability capacitance retention and rate performance of the synthesized material was tested by running 7000 cycles at $20Ag^{-1}$. NCO/NCSe//AC exhibited excellent cyclic performance by retaining 116% of capacitance at 20 A g-1 over 7000 charge-discharge cycles indication much better durability as shown in Figure 5.13 whereas columbic efficiency remains 99% throughout the cycles. The extraordinary performance of NCO/NCSe can be ascribed to its novel mesoporous core/shell assembly and the bimetallic synergistic effect. Firstly, the mesoporous structure increases surface area and number of active sites and also shortens the ion/electron pathways. Secondly the interconnected nanowires structure with high electron mobility improves the rate performance and reversibility of the material by lowering the equivalent series resistance and charge-transfer resistance. Finally, bimetallic's synergistic effect aids in improving conductivity and electrochemical active sites, resulting in high-rate capability and capacitance

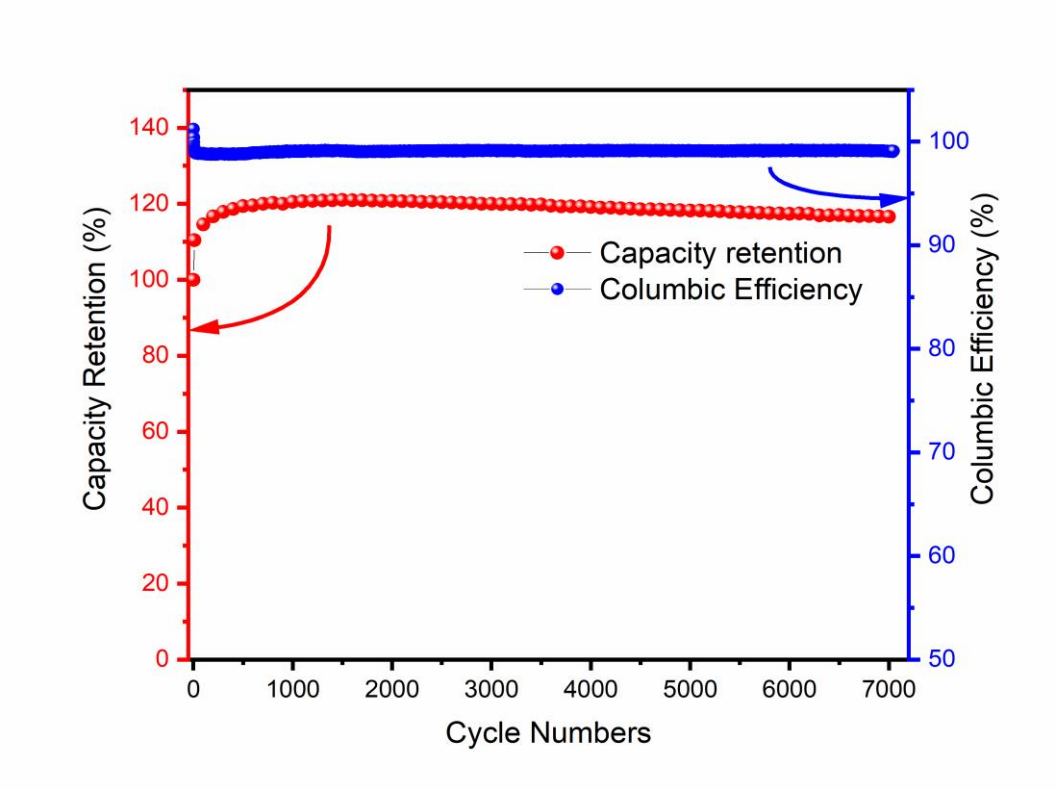

figure 5.13 Cyclic performance of asymmetric device

The synthesized NCO/NCSe //AC possesses superior electrochemical properties and hence it can be used in different energy devices in order to meet the recent energy demands and tailor new materials. One of the desired materials for the upcoming electrochemical devices might be the produced material owing to its excellent properties.

Conclusion

The properties of the super-capacitors are determined by kind of electrode material used and hence structure and morphology of the material are to be considered as well. Usually, the hollow structures, especially the complex ones are known to introduce remarkable properties as they have structural robustness and unique features. The idea of developing porous chemistries that allow quick mass diffusion has been presented as a result of recent advances in morphologies. Creating hierarchically porous interactions to enhance electrode/electrolyte interface having superior jurisdiction over mixed metal oxide conformation is somewhat quite thought-provoking. It is believed that the existence of meso and micropores promotes rapid mass diffusion and improved electrode/electrolyte interaction. Therefore, to achieve the highest specific capacitance with a longer cyclic life, it is essential to synthesize mixed metal selenide nanostructures with extraordinary control over the structure; nevertheless, it is challenging to achieve specific morphologies since the structure eventually disintegrates.

For our work, we have tried different approaches to achieve specific structure. Firstly, we tried selenization by hydrothermal method but the results from SEM indicated that the structure got disintegrated and we couldn't achieve our required morphology. Secondly, we employed tube furnace selenization to attain mesophorous nanowires structure for our material, but the results showed that the morphology was yet again degenerated. Lastly, NCO//NCSe (Core/shell) mesoporous nanowires were manufactured using a facile hydrothermal approach after utilizing wet chemistry method for selenization.

The manufactured needle like nanowires exhibit much greater surface area which results in extraordinary electrochemical functioning because of the boost in electrode/electrolyte Interface. The mesopores within the nanowires provided shorter diffusion pathways which lead to performance of reversible operation at higher charge/discharge rates. Since the Mesoporous nanowires possess novel nanowires assembly the material delivered exceptional capacitive performance.

Nickel Cobalt oxide@Nickel cobalt Selenide core/shell morphology was examined by SEM. SEM analysis of NCO/NCSe shows the hierarchical nanostructures. Nanowires

are arranged in one direction which affirmed the porous nature of the material as well as good transport of electrolyte during an electrochemical performance. The crystal structure of the material was recorded by employing XRD and to analyze the specific surface area of the material BET surface area analyzer was used. Electrochemical analysis affirmed the developed hierarchically mesoporous NCSe//NCO nanowires for supercapacitors and all the electrochemical tests were accompanied at room temperature using a Biologic VSP electrochemical workstation. The traditional slurry-coating method was used for the preparation of working electrode.

NCSe //NCO nanowires exhibited a specific capacitance of 3281.54 F g^{-1} at 1 Ag^{-1}. Moreover, asymmetric testing by employing NCSe //NCO as positive electrode and Activated Carbon as a negative electrode. All the tests were conducted at a broad operational window of 0 V to 1.5 V. The charge balance between the positive and negative electrodes strongly influenced the performance of asymmetric supercapacitor. The asymmetric supercapacitor (ASC) with activated carbon shows high energy density 37.91 Wh kg^{-1} at a power density of 749.95W kg^{-1} and excellent capacitance retention of 116% over 7000 cycles with columbic efficiency of 99% at 20 Ag^{-1}.

References

[1] Gielen, D., et al., *The role of renewable energy in the global energy transformation.* Energy Strategy Reviews, (2019). **24**: p. 38-50.

[2] Glassmeyer, S.T., et al., *Nationwide reconnaissance of contaminants of emerging concern in source and treated drinking waters of the United States.* Science of The Total Environment, (2017). **581-582**: p. 909-922.

[3] de Fraiture, C., M. Giordano, and Y. Liao, *Biofuels and implications for agricultural water use: blue impacts of green energy.* Water Policy, (2008). **10**(S1): p. 67-81.

[4] Zhu, K., et al., *Fast synthesis of uniform mesoporous titania submicrospheres with high tap densities for high-volumetric performance Li-ion batteries.* Science China Materials, (2017). **60**(4): p. 304-314.

[5] Miller, E.E., Y. Hua, and F.H. Tezel, *Materials for energy storage: Review of electrode materials and methods of increasing capacitance for supercapacitors.* Journal of Energy Storage, (2018). **20**: p. 30-40.

[6] González, A., et al., *Review on supercapacitors: Technologies and materials.* Renewable and Sustainable Energy Reviews, (2016). **58**: p. 1189-1206.

[7] Wang, F., et al., *Latest advances in supercapacitors: from new electrode materials to novel device designs.* Chemical Society Reviews, (2017). **46**(22): p. 6816-6854.

[8] O'Neill, A., U. Khan, and J.N. Coleman, *Preparation of High Concentration Dispersions of Exfoliated MoS2 with Increased Flake Size.* Chemistry of Materials, (2012). **24**(12): p. 2414-2421.

[9] Li, X., et al., *Orderly Integration of Porous TiO2(B) Nanosheets into Bunchy Hierarchical Structure for High-Rate and Ultralong-Lifespan Lithium-ion Batteries.* Nano Energy, (2017). **31**: p. 1-8.

[10] Kim, B.K., et al.

[11] Shanmugam, S.R., S. Adhikari, and R. Shakya, *Nutrient removal and energy production from aqueous phase of bio-oil generated via hydrothermal liquefaction of algae.* Bioresource technology, (2017). **230**: p. 43-48.

[12] Sani, A.K., et al., *A review on the performance of geothermal energy pile foundation, its design process and applications.* Renewable and Sustainable Energy Reviews, (2019). **106**: p. 54-78.

[13] Bahadur, N., et al., *Rapid synthesis, characterization and optical properties of TiO2 coated ZnO nanocomposite particles by a novel microwave irradiation method.* Materials Research Bulletin, (2010). **45**: p. 1383-1388.

[14] Ko, K.H., Y.C. Lee, and Y.J. Jung, *Enhanced efficiency of dye-sensitized TiO2 solar cells (DSSC) by doping of metal ions.* J Colloid Interface Sci, (2005). **283**(2): p. 482-7.

[15] Gebraad, P., et al., *Maximization of the annual energy production of wind power plants by optimization of layout and yaw-based wake control: Maximization of wind plant AEP by optimization of layout and wake control.* Wind Energy, (2016). **20**.

[16] Sluiter, A., et al., *Determination of structural carbohydrates and lignin in biomass, in: Laboratory Analytical Procedure (LAP).* National Renewable Energy Laboratory, (2008)

[17] Huber, G.W., S. Iborra, and A. Corma, *Synthesis of Transportation Fuels from Biomass: Chemistry, Catalysts, and Engineering.* Chemical Reviews, (2006). **106**(9): p. 4044-4098.

[18] Dehghani-Sanij, A.R., et al., *Study of energy storage systems and environmental challenges of batteries.* Renewable and Sustainable Energy Reviews, (2019). **104**: p. 192-208.

[19] Alva, G., Y. Lin, and G. Fang, *An overview of thermal energy storage systems.* Energy, (2018). **144**: p. 341-378.

[20] May, G.J., A. Davidson, and B. Monahov, *Lead batteries for utility energy storage: A review.* Journal of Energy Storage, (2018). **15**: p. 145-157.

[21] Zhang, C., et al., *Energy storage system: Current studies on batteries and power condition system.* Renewable and Sustainable Energy Reviews, (2018). **82**: p. 3091-3106.

[22] Cao, X., et al., *Preparation of Novel 3D Graphene Networks for Supercapacitor Applications.* Small, (2011). **7**(22): p. 3163-3168.

[23] Siwatch, P., et al., *Review of supercapacitors: Materials and devices.* Journal of Energy Storage, (2019). **21**: p. 801-825.

[24] Vangari, M., T. Pryor, and L. Jiang, *Supercapacitors: Review of Materials and Fabrication Methods.* Journal of Energy Engineering, (2013). **139**(2): p. 72-79.

[25] Xu, J., et al., *Preparation and electrochemical capacitance of cobalt oxide (Co 3O 4) nanotubes as supercapacitor material.* Electrochimica Acta - ELECTROCHIM ACTA, (2010) **56**: p. 732-736.

[26] Kandasamy, S.K. and K. Kandasamy, *Recent Advances in Electrochemical Performances of Graphene Composite (Graphene-Polyaniline/Polypyrrole/Activated Carbon/Carbon Nanotube) Electrode Materials for Supercapacitor: A Review.* Journal of Inorganic and Organometallic Polymers and Materials, (2018). **28**: p. 559-584.

[27] Azman, N.H.N., et al., *Graphene-based ternary composites for supercapacitors.* International Journal of Energy Research, (2018). **42**(6): p. 2104-2116.

[28] Wang, H., J. Lin, and Z.X. Shen, *Polyaniline (PANi) based electrode materials for energy storage and conversion.* Journal of Science: Advanced Materials and Devices, (2016). **1**(3): p. 225-255.

[29] Eftekhari, A., L. Li, and Y. Yang, *Polyaniline supercapacitors.* Journal of Power Sources, (2017). **347**: p. 86-107.

[30] Kumar, S., et al., *Carbon-polyaniline nanocomposites as supercapacitor materials.* Materials Research Express, (2018). **5**: p. 045505.

[31] Lee, S.-Y., J.-I. Kim, and S.-J. Park, *Activated carbon nanotubes/polyaniline composites as supercapacitor electrodes.* Energy, 2014. **78**: p. 298-303.

[32] Huang, Y., et al., *Nanostructured Polypyrrole as a flexible electrode material of supercapacitor.* Nano Energy, (2016). **22**: p. 422-438.

[33] Chee, W.K., H.N. Lim, and N.M. Huang, *Electrochemical properties of free-standing polypyrrole/graphene oxide/zinc oxide flexible supercapacitor.* International Journal of Energy Research, (2015). **39**(1): p. 111-119.

[34] Poizot, P., et al., *Nano-sized transition-metal oxides as negative-electrode materials for lithium-ion batteries.* Nature, (2000). **407**(6803): p. 496-499.

[35] Chhowalla, M., et al., *The chemistry of two-dimensional layered transition metal dichalcogenide nanosheets.* Nat Chem, (2013). **5**(4): p. 263-75.

[36] Matnishyan, H., et al., *Synthesis and study of polyaniline nanocomposites with metal oxides.* Physics of the Solid State, (2011). **53**.

[37] Alqahtani, D.M., et al., *Effect of metal ion substitution on electrochemical properties of cobalt oxide.* Journal of Alloys and Compounds, (2019). **771**: p. 951-959.

[38] Kouchachvili, L., W. Yaïci, and E. Entchev, *Hybrid battery/supercapacitor energy storage system for the electric vehicles.* Journal of Power, (2018). **374**: p. 237–248.

[39] Mei, J., et al., *Cobalt oxide-based nanoarchitectures for electrochemical energy applications.* Progress in Materials Science, (2019). **103**: p. 596-677.

[40] Hua, Y., et al., *Cobalt based metal-organic frameworks and their derivatives for electrochemical energy conversion and storage.* Chemical Engineering Journal, (2019). **370**: p. 37-59.

[41] Qi, S., et al., *Cobalt-based electrode materials for sodium-ion batteries.* Chemical Engineering Journal, (2019). **370**: p. 185-207.

[42] Chen, M., et al., *Cobalt oxides nanorods arrays as advanced electrode for high performance supercapacitor.* Surface and Coatings Technology, (2019). **360**: p. 73-77.

[43] Chen, T.-Y. and L.-Y. Lin, *Morphology variation for the nickel cobalt molybdenum copper oxide with different metal ratios and their application on energy storage.* Electrochimica Acta, (2019). **298**: p. 745-755.

[44] Alcántara, R., et al., *NiCo2O4 Spinel: First Report on a Transition Metal Oxide for the Negative Electrode of Sodium-Ion Batteries.* Chemistry of Materials, (2002). **14**(7): p. 2847-2848.

[45] Yuan, Y.F., et al., *Hierarchically porous Co 3O 4 film with mesoporous walls prepared via liquid crystalline template for supercapacitor application.* Electrochemistry Communications - ELECTROCHEM COMMUN, (2011). **13**: p. 1123-1126.

[46] Kung, C.-W., et al., *Synthesis of Co3O4 nanosheets via electrodeposition followed by ozone treatment and their application to high-performance supercapacitors.* Journal of Power Sources, (2012). **214**: p. 91-99.

[47] Fan, Y., et al., *Ultrathin Nanoflakes Assembled 3D Hierarchical Mesoporous Co3O4 Nanoparticles for High-Rate Pseudocapacitors.* Particle & Particle Systems Characterization, (2014). **31**(10): p. 1079-1083.

[48] Zhang, G., et al., *Nanoforest of hierarchical Co3O4@NiCo2O4 nanowire arrays for high-performance supercapacitors.* Nano Energy, (2013). **2**(5): p. 586-594.

[49] Huang, M., et al., *Facile synthesis of hierarchical Co3O4@MnO2 core–shell arrays on Ni foam for asymmetric supercapacitors.* Journal of Power Sources, (2014). **252**: p. 98-106.

[50] Huang, T., et al., *Facilely synthesized porous ZnCo2O4 rodlike nanostructure for high-rate supercapacitors.* Ionics, (2015). **21**: p. 3109-3115.

[51] Zhang, C., et al., *Facile preparation of flower-like NiCo2O4/three dimensional graphene foam hybrid for high performance supercapacitor electrodes.* Carbon, (2015). **89**: p. 328-339.

[52] Chen, H., et al., *3D hierarchically porous zinc–nickel–cobalt oxide nanosheets grown on Ni foam as binder-free electrodes for electrochemical energy storage.* Journal of Materials Chemistry A, (2015). **3**(47): p. 24022-24032.

[53] Ma, W., et al., *Superior performance asymmetric supercapacitors based on ZnCo2O4@MnO2 core–shell electrode.* Journal of Materials Chemistry A, (2015). **3**(10): p. 5442-5448.

[54] Xu, K., et al., *Hierarchical mesoporous NiCo2O4@MnO2 core–shell nanowire arrays on nickel foam for aqueous asymmetric supercapacitors.* Journal of Materials Chemistry A, (2014). **2**(13): p. 4795-4802.

[55] Liu, X., J. Liu, and X. Sun, *NiCo2O4@NiO hybrid arrays with improved electrochemical performance for pseudocapacitors.* Journal of Materials Chemistry A, (2015). **3**(26): p. 13900-13905.

[56] Xu, Y., et al., *Facile synthesis route of porous MnCo2O4 and CoMn2O4 nanowires and their excellent electrochemical properties in supercapacitors.* Journal of Materials Chemistry A, (2014). **2**(39): p. 16480-16488.

[57] Xu, Y., et al., *Mesoporous composite nickel cobalt oxide/graphene oxide synthesized via a template-assistant co-precipitation route as electrode material for supercapacitors.* Journal of Power Sources, (2016). **306**: p. 742-752.

[58] Sahoo, S. and J.-J. Shim, *Facile Synthesis of Three-Dimensional Ternary ZnCo2O4/Reduced Graphene Oxide/NiO Composite Film on Nickel Foam for Next Generation Supercapacitor Electrodes.* ACS Sustainable Chemistry & Engineering, (2017). **5**(1): p. 241-251.

[59] Fang, L., et al., *Hierarchical CoMoO4 nanoneedle electrodes for advanced supercapacitors and electrocatalytic oxygen evolution.* Electrochimica Acta, (2018). **259**: p. 552-558.

[60] Hu, W., et al., *Flower-like nickel-zinc-cobalt mixed metal oxide nanowire arrays for electrochemical capacitor applications.* Journal of Alloys and Compounds, (2017) **708**: p. 146-153.

[61] Wu, C., et al., *Hybrid Reduced Graphene Oxide Nanosheet Supported Mn-Ni-Co Ternary Oxides for Aqueous Asymmetric Supercapacitors.* ACS applied materials & interfaces, (2017). **9**.

[62] Zhao, J., et al., *Hierarchical ferric-cobalt-nickel ternary oxide nanowire arrays supported on graphene fibers as high-performance electrodes for flexible asymmetric supercapacitors.* Nano Research, (2018). **11**(4): p. 1775-1786.

[63] He, X., et al., *Hierarchical FeCo2O4@NiCo layered double hydroxide core/shell nanowires for high performance flexible all-solid-state asymmetric supercapacitors.* Chemical Engineering Journal, (2018). **334**: p. 1573-1583.

[64] Feng, H., et al., *Construction of 3D hierarchical porous NiCo2O4/graphene hydrogel/Ni foam electrode for high-performance supercapacitor.* Electrochimica Acta, (2019). **299**: p. 116-124.

[65] Li, Z.-Y., et al., *Enhanced electrochemical activity of low temperature solution process synthesized Co3O4 nanoparticles for pseudo-supercapacitors applications.* Ceramics International, (2016). **42**(1, Part B): p. 1879-1885.

[66] Jittiarporn, P., et al., *Electrochromic properties of sol–gel prepared hybrid transition metal oxides – A short review.* Journal of Science: Advanced Materials and Devices, (2017). **2**(3): p. 286-300.

[67] Yang, Q., et al., *Metal oxide and hydroxide nanoarrays: Hydrothermal synthesis and applications as supercapacitors and nanocatalysts.* Progress in Natural Science: Materials International, (2013). **23**(4): p. 351-366.

[68] Emadi, H., M. Salavati-Niasari, and A. Sobhani, *Synthesis of some transition metal (M: 25Mn, 27Co, 28Ni, 29Cu, 30Zn, 47Ag, 48Cd) sulfide nanostructures by hydrothermal method.* Advances in colloid and interface science, (2017). **246**: p. 52-74.

[69] Li, Q., et al., *Synthesis and characterization of shape-controlled Ni0.5Zn0.5Fe2O4 via the coprecipitation method.* Journal of Alloys and Compounds, (2010). **495**(1): p. 63-66.

[70] Margulis-Goshen, K. and S. Magdassi, *Organic nanoparticles from microemulsions: Formation and applications.* Current Opinion in Colloid & Interface Science, (2012). **17**(5): p. 290-296.

[71] Gaur, A.P.S., et al., *Surface Energy Engineering for Tunable Wettability through Controlled Synthesis of MoS2.* Nano Letters, (2014). **14**(8): p. 4314-4321.

[72] Li, H., et al., *Preparation and applications of mechanically exfoliated single-layer and multilayer MoS_2 and WSe_2 nanosheets.* Acc Chem Res, (2014). **47**(4): p. 1067-75.

[73] Matsunaga, T., et al., *Photoelectrochemical sterilization of microbial cells by semiconductor powders.* FEMS Microbiology Letters, (1985). **29**(1-2): p. 211-214.

[74] Li, H., et al., *Fabrication of Single- and Multilayer MoS2 Film-Based Field-Effect Transistors for Sensing NO at Room Temperature.* Small, (2012). **8**(1): p. 63-67.

[75] Shen, J., et al., *Liquid Phase Exfoliation of Two-Dimensional Materials by Directly Probing and Matching Surface Tension Components.* Nano Letters, (2015). **15**(8): p. 5449-5454.

[76] Gupta, A., V. Arunachalam, and S. Vasudevan, *Water Dispersible, Positively and Negatively Charged MoS2 Nanosheets: Surface Chemistry and the Role of Surfactant Binding.* The Journal of Physical Chemistry Letters, (2015). **6**(4): p. 739-744.

[77] Cunningham, G., et al., *Solvent Exfoliation of Transition Metal Dichalcogenides: Dispersibility of Exfoliated Nanosheets Varies Only Weakly between Compounds.* ACS nano, (2012). **6**: p. 3468-80.

[78] Jerosch, J. and R. Reichelt, *[Scanning electron microscopy studies of morphologic changes in chemically stabilized ultrahigh molecular weight polyethylene]*. Biomed Tech (Berl), (1997). **42**(12): p. 358-62.

[79] Joy, D.C. and J.B. Pawley, *High-resolution scanning electron microscopy.* Ultramicroscopy, (1992). **47**(1): p. 80-100.

[80] Schmitt, R., *Scanning Electron Microscope*, in *CIRP Encyclopedia of Production Engineering*, L. Laperrière and G. Reinhart, Editors. (2014), Springer Berlin Heidelberg: Berlin, Heidelberg. p. 1085-1089.

[81] Naderi, M., *Chapter Fourteen Surface Area Brunauer–Emmett–Teller (BET)*, in *Progress in Filtration and Separation*. (2015). p. 585-608.